

AD



WAL TR 834.2/3

WATERTOWN ARSENAL LABORATORIES

RELATIONSHIPS BETWEEN ENERGY, FIBROSITY AND
TEMPERATURE IN CHARPY IMPACT TESTS ON AISI 4340 STEEL

TECHNICAL REPORT NO. WAL TR 834.2/3

BY

FRANK R. LARSON

AND

JOHN NUNES

DATE OF ISSUE - DECEMBER 1961

OMS CODE 5010.11.8420051

RESEARCH OF METALS AND NONMETALLIC MATERIALS FOR ORDNANCE CONSTRUCTION

D/A PROJECT 593-32-002

WATERTOWN ARSENAL
WATERTOWN 72, MASS.

AD

Plastic flow
and fracture
Testing -
Charpy impact

RELATIONSHIPS BETWEEN ENERGY, FIBROSITY AND
TEMPERATURE IN CHARPY IMPACT TESTS ON AISI 4340 STEEL

Technical Report No. WAL TR 834.2/3

Frank R. Larson
and
John Nunes

45652

Date of Issue - December 1961

OMS Code 5010.11.8420051
Research of Metals and Nonmetallic Materials for Ordnance Construction
D/A Project 593-32-002

WATERTOWN ARSENAL
WATERTOWN 72, MASS.


WATERTOWN ARSENAL LABORATORIES

TITLE

RELATIONSHIPS BETWEEN ENERGY, FIBROSITY AND
TEMPERATURE IN CHARPY IMPACT TESTS ON AISI 4340 STEEL

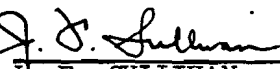
ABSTRACT

A study was conducted on the relationships between impact energy, percent fibrosity and test temperature in the Charpy tests for AISI 4340 steel. It is shown that a linear function of percent fibrosity versus energy exists. Also an energy value (U_F) derived from this function is shown to be related to basic strain-hardening properties. Furthermore, a relationship, based upon the rate of change in U_F with respect to temperature, was established. Finally, it was possible to describe the appearance of the fracture by identifying three regions of behavior, namely, shear lip, center fibrous, and flat. The flat region can be considered representative of rapid fracture while the center fibrous would indicate slow ductile fracture, rapid and slow being defined in this study by unstable and stable fracture propagation.


FRANK R. LARSON
Supervisory Physical Metallurgist


JOHN NUNES
Materials Engineer

APPROVED:


J. F. SULLIVAN
Director
Watertown Arsenal Laboratories

CONTENTS

	Page
ABSTRACT	
INTRODUCTION	3
MATERIAL AND PROCEDURE	4
RESULTS AND DISCUSSION	
Energy-Fibrosity Relationship	4
Temperature (Transitional Behavior)	6
Energy Ductility Relationship	7
SUMMARY	8
TABLES	10
ILLUSTRATIONS	18
APPENDIX	48
REFERENCES	49

INTRODUCTION

Over the years metallurgists and engineers have examined the fractured surfaces of failed structures or components for evidence of cause, since it has been known for a long time that an examination of a fracture can provide a great deal of information about the cause and history of the failure.^{1,2} One of the most important facts revealed by such a study, at least for steels, is that a determination of the type of fracture, whether it be brittle or ductile, is practicable. This determination can be done easily for there is a marked difference, especially at low strength levels, in the appearance of the ductile and brittle fracture surfaces. The main interest in fracture surfaces probably arose from the general observation that crystalline fractures are most likely to be present in failures that are catastrophic and unpredictable and therefore should be avoided.

The main upswing in interest in fracture surface appearance by researchers, at least in this country, occurred around 1945^{3,4,5} and this was probably brought about by World War II experiences with service failures. There has been a large number of different types of tests employed in the laboratory, designed specifically to study the toughness of materials, but there seems to be no general acceptance of any one type although the use of the Charpy (V-notch) test appears to be more widespread than any other.

One of the principal uses of these toughness tests is the determination of the ductile-to-brittle transition behavior as the testing temperature is varied. In reality, this behavior change occurs over a temperature range but, for convenience, one specific temperature in this range is chosen and called "the transition temperature". There are several criteria used to define the transition temperature. Some are based on energy and others based on fracture surface appearances.⁶ There has also been some recent interest in other criteria which are based upon ductility.^{7,8} It is apparent that the dilemma arises primarily from the fact that each method seems to give different results as to both transition temperature and the relative order of toughness among various materials.

A great deal of light could be shed upon this problem by studying the interrelationships between some of these phenomena. After a study of several sets of data, it became apparent that energy and fracture appearance seem to be related. This observation was also made by previous investigators^{5,9} in this country but failure to obtain correlations was probably due to insufficient precision in measurement of various regions of the fracture surfaces. In recent investigations abroad,^{10,11} low-strength carbon steels showed a reasonable correlation between fracture appearance and energy absorbed. [It was the purpose of this investigation to study the relationships between impact energy and fracture surface appearance on a heat-treated alloy steel at various strength levels and microstructures. Some attempt was also made to compare the above

relationships to the strain-hardening properties of the SAE 4340 steel as determined in the tension test.]

MATERIAL AND PROCEDURE

The chemical composition of the single heat of 9/16" square SAE 4340 bar used in this investigation is listed in Table I. This hot-rolled annealed bar was cut into blanks 2-1/8" long and then heat treated according to procedures listed in Table II. Representative heat-treated microstructures are illustrated in Figures 1 through 5.

[Standard Charpy V-notch specimens were machined and then tested in impact over a range of temperatures in order to obtain the typical transition curves.

The energy to fracture the bars and the percent fibrous area on the fractured surfaces were determined and are recorded in Tables III through XIV. The percent fibrous area for some groups was rated by two methods, one of which was the usual visual estimate. The second method involved photographing the broken bars, at approximately 20X magnification, measuring the nonfibrous and total areas with a planimeter and then computing the relative percentages. Figures 6 through 9 illustrate typical photographs of fracture surfaces upon which the planimeter readings were made. These test results are portrayed in conventional plots for impact energy and percent fibrosity vs. testing temperatures in Figures 10 through 21.

RESULTS AND DISCUSSION

Energy-Fibrosity Relationship

It has been known for many years, as pointed out by previous investigators,^{10,11} that there is a general correlation between fracture surface appearance and the energy absorbed in rupturing impact specimens. For example, when one develops an energy and fibrosity curve as a function of testing temperature, it is usually found that a plateau of nearly constant energy exists at the upper testing temperatures for 100 percent fibrous fracture. The percent fibrosity decreases with lowered testing temperature, and the energy also decreases with it. However, superficial examination soon reveals that one-to-one relationship does not exist between these two variables. For example, if the 100 percent fibrosity energy is at 20 foot-pounds, the 50 percent fibrosity energy may not be 10 foot-pounds but is probably around 15 foot-pounds. A literature survey revealed that two German workers (Schepers and Licht¹⁰ and Kornfeld¹¹) studied this problem. They show plots of energy versus fibrosity and arrive at the conclusion that there is a linear relationship, at least for their material, which was a mild steel.

[Utilizing the data contained in Figures 10 through 21, graphs were constructed plotting the impact energy versus the percent fibrosity. The curves obtained are illustrated in Figures 22 to 26. Examination of these figures reveals that, over a range of values, a reasonably linear relationship exists between the energy and fibrosity parameters.] Scatter of the data points is relatively small for those points measured with the planimeter. However, as the visual readings are seldom better than ± 5 percent, the scatter for these data tends to be much larger. Even in the light of this observation, a relatively good trend is evident.

[From the observed trend, there appear to be two regions of behavior. The higher values of fibrosity, ranging from 100 percent to approximately 10 percent, is the region of best correlation and it is this region that will be dealt with primarily in this report. At lower values of fibrosity, there is an inflection point at approximately 10 percent fibrosity and the data seem to follow a general trend toward zero percent fibrosity and energy.] The extrapolation of the linear line, from above 10 percent fibrosity, results in a positive energy intercept at zero percent fibrosity. Below 10 percent fibrosity, the shear lip, the only remaining fibrous area, begins to decrease in size and the energy-fibrosity curve changes slope to approach zero.

Examination of the data reveals that, by representing the energy values in a percentage form, it is possible to obtain a straight-line relationship with the percent fibrosity. One method for accomplishing this is illustrated in Appendix A. In representing the energy values as percentages, it is first necessary to establish two quantities: (1) the lowest energy value for a 100 percent fibrous fracture (U_{100}), and (2) the energy intercept at zero fibrosity (U_0), from the energy versus fibrosity plots (Figures 22 through 26). The results of these calculations are given by Table XV.

As shown by Appendix A, the difference between U_{100} and U_0 is designated U_F . Now, various points on the transition curves of Figures 10 through 21 can be represented as percentages of U_F . [When these percentages are plotted versus percent fibrosity the result is a straight line, as shown by Figure 27, and the slope of this line is 1.]

In this plot, the solid points represent those which were read with a planimeter while the open points are the visual estimates. It can readily be seen, as might be expected, that the planimeter points are generally closer to the trend line and more uniformly distributed. However, there is some scatter which is rather difficult to explain. This scatter occurs primarily in the high strength level specimens where the determination of zero and 100 percent fibrosity energy levels (U_0 and U_{100}) is fairly critical.

The steep slope of the energy versus fibrosity plots of the U, T and D series (Figure 22) should be noted. These are the heat treatments that give the greatest scatter. Since the given energy is much lower, then a small error in each individual test point would show up as a large percentage error on this graph. The error would be approximately 20

percent for 1 foot-pound.

A few comments should be made about U_0 , the energy intercept of the percent fibrosity-energy plots. One might expect that this should be zero rather than a value between 5 and 17 foot-pounds. However, it is considered that this value is energy which is not directly involved in the specimen fracture. It involves the energy of compression deformation of the specimen caused by the tup and anvils.

Temperature (Transitional Behavior)

As has been previously indicated, some of the confusion in the use of testing procedures that bring about transitions in behavior arises because of the difficulty in selecting a single parameter which describes these phenomena. These transitions are a result of a bi-modal and a tri-modal behavior over a range of temperature. For the impact transition, it is apparent that this is the problem. In these tests it is clear that there are at least three regions of different behavior patterns.

Beginning at high testing temperatures, the high-level impact energy gradually decreases with decreasing testing temperature. At the lower testing temperatures, the same trend of slow decrease in impact energy occurs but at a much lower energy level. (See Figure 28). The changes in impact energy in these cases seem to be due primarily to relatively slow changes in the size of the shear lips on the sides and the back of the specimen. At temperatures in the region between these two extremes, there is a sharp drop in energy. In this region of tri-modal behavior, the drop in impact energy is primarily associated with the growth of an area near the center of the specimen which is designated in this report as "flat". It has been generally called "the crystalline area" or sometimes "cleavage fracture". There seems to be some question as to whether or not it is cleavage, especially for tempered martensite. Studies of the fracture surfaces of these and other specimens leave considerable doubt that the center areas of tri-modal fractures are cleavage for the martensite. However, it may be cleavage for the pearlite and the bainite studied here. These considerations, although not essential to this discussion, are important.

It is evident that these center areas have relatively flat surfaces and represent small plastically deformed volumes of metal and hence are low-energy absorbing. The important point is that this flat, low-energy absorbing center area grows at the expense of the fibrous area.

One of the possible criteria for use in comparing materials with respect to transitional behavior is, of course, the lowest temperature at which 100 percent fibrosity persists. This temperature is fairly easy to determine, is quite frequently used and may have considerable basic significance. Although further studies are needed and are under way, results obtained in this program clarify some of the problems with regard to the abruptness of the energy transition. One of the major concerns of investigators, using the impact test to evaluate brittle-to-ductile

behavior, has centered around the abruptness of this transition.

[From the energy-fibrosity relationships previously established, in addition to a visual examination of the broken specimens, it can be seen that the major portion of the energy drop depends upon the growth of the fracture area.] Now, the abruptness of the energy drop depends upon the difference between the 100% fibrosity energy (U_{100}) and the zero percent fibrosity energy intercept (U_0) along with the temperature range over which this change occurs. More simply, it is the slope of the energy versus testing temperature curve in the region of 100 percent to approximately 20 percent fibrosity.

[Referring back to Figures 10 through 22, it can be seen that it is possible to draw reasonably straight lines through the energy-temperature plots in this region. It would also follow, from energy-fibrosity relationships established in this report, that a similar straight line could be drawn through the fibrosity-temperature plots. It then appears that two important features of the ductile-to-brittle transitional behavior can be inferred from the preceding discussion. Figure 29 illustrates this for the heat treatments employed in this study.

In this Figure 29, the slope (foot-pounds/degree Centrigade) of the energy-temperature curve is plotted versus the lowest temperature at which the specimen is still 100 percent fibrous (TT_{100}). From this figure, it can be seen that the various microstructures are separated. Furthermore, the relative behavior of tempered martensite, as a function of tempering treatment or hardness level, is also illustrated. At high hardness, the transition temperature is high and the energy drop with decreasing testing temperature is very gradual. As the hardness decreases, the transition temperature is lowered and the ductile-to-brittle energy drop becomes more abrupt. The bainite and pearlite both seem to follow the same general pattern. Another way of viewing the data is that, for a given microstructure, the transition temperature decreases with the increasing steepness of the energy versus temperature slope in the energy-fibrosity transition range.]

Energy-Ductility Relationship

Normally it is not desirable to use heat-treated steels for service at temperatures below their transition temperature, i.e., for maximum safety these materials should be used only above this transition temperature. Therefore, it would be useful to be able to estimate the relative level of toughness from another type of test, such as the tension test. Such an evaluation would also be valuable in fostering a basic understanding of impact tests, although it is realized that this approach is somewhat open to criticism, particularly because of a lack of complete stress and strain analysis during the plastic flow associated with the rupturing of impact test bars. However, it is felt that an empirical approach, guided by some elementary reasoning, would be useful.

Plastic deformation that develops during the straining of any specimen

depends upon the work-hardening or strain-hardening properties of the material being deformed. More specifically, the strain-hardening properties control the extent of uniform deformation in tension testing and in most stretching operations. In these cases it is the work-hardening properties that resist local or necking deformation. For bending, notches and conditions that cause strain gradients during plastic deformation, it is the strain-hardening properties that tend to prevent localization of plastic strain. A material with high strain-hardening will have a large volume of material participating in the deformation and hence should have high toughness. These remarks would apply only to the ductile fracture case, of course. There are many other factors that influence the impact energy of fracture, so that caution should be used in trying to apply these general principles.

It is evident from the foregoing discussion that strain-hardening and those properties that are dependent upon it should correlate. To test these ideas, Figure 30 was constructed. In this graph, the strain-hardening exponent n , determined from true stress-strain tension tests at room temperature, was plotted against the impact energy value U_F . Since the elongation depends in part upon the strain-hardening exponent, it too was plotted versus the impact energy. Notice the strong dependence of the ductile impact energy upon the ductility and strain-hardening exponent.

SUMMARY

From the results obtained in this investigation on AISI 4340 steel heat treated to various microstructures and strength levels, it has been shown that:

1. There is a linear relationship between percent fibrosity and energy of fracture in impact.
2. It appears that it is possible to explain fairly accurately the shape of the impact energy and fibrosity plots versus temperature by an identification of the three regions of fracture, each of which is characteristic of certain fracturing behavior.
3. Using the lowest temperature at which 100 percent fibrosity exists as the transition temperature, fracture surface studies have shown that - above this temperature, two fracture surfaces were present: (a) flat fibrous center, and (b) shear lip edges; below this temperature, the center fibrous area begins to change to a very flat surface and, in an intermediate range, three fracture surfaces are present. At the lowest temperatures, only two fracture modes were present: a very flat surface and a shear lip.
4. For the martensite, higher tempering temperatures produced lower transition temperatures, with the lowest occurring at a 1100 F temper. Along with this lower transition temperature, a more abrupt energy decrease occurred in the transition range.

5. Both of the pearlitic and bainitic structures tested here showed higher transition temperatures than the martensite for equivalent energy or strength level.

6. Finally, it was shown that the energy U_F is related to the basic strain-hardening properties in tension and hence is related to the ductility expressed in elongation.

↓
—

TABLE I

CHEMICAL COMPOSITION (wt. %)

C	Mn	Si	S	P	Ni	Cr	Mo
0.375 to 0.385	0.73 to 0.77	0.32 to 0.33	0.020 to 0.023	0.008 to 0.009	1.75 to 1.80	0.79 to 0.80	0.24 to 0.26

TABLE II

HEAT TREATMENT, SAE 4340 STEEL

Series		Normalize	Austenitize	Temper	Stress Relief
D	M A R T E N S I T E		1525 F 1 hr	Marquenched 430 F (hot salt) 5 min, air cooled, 765 F 2 hr, oil quenched	
E		1650 F 1 hr, air cooled	1600 F 1 hr, oil quenched	1035 F 1½ hr, oil quenched	570 F 3 hr, air cooled
F		1650 F 1 hr, air cooled	1600 F 1 hr, oil quenched	1250 F 1½ hr, water quenched	570 F 3 hr, air cooled
P		1650 F 1 hr, air cooled	1600 F 1 hr, oil quenched	1100 F 1½ hr, water quenched	570 F 3 hr, air cooled
S		1650 F 1 hr, air cooled	1600 F 1 hr, oil quenched	900 F 1½ hr, water quenched	570 F 3 hr, air cooled
T		1650 F 1 hr, air cooled	1600 F 1 hr, oil quenched	500 F 1½ hr, water quenched	
U		1650 F 1 hr, air cooled	1600 F 1 hr, oil quenched	500 F 1½ hr, double temper, water quenched	
M and N	P E A R L I T E	1650 F 1 hr, air cooled	1550 F 4 hr	Slow cooled to 1200 F 48 hr, furnace cooled	
O		1650 F 1 hr, air cooled	1550 F 4 hr	Slow cooled to 1100 F 48 hr, furnace cooled	
J	B A I N I T E		1550 F 1½ hr	740 F (hot salt) 24 hr, oil quenched	
K			1550 F 1½ hr	650 F (hot salt) 4 hr, oil quenched	

TABLE III

IMPACT TEST RESULTS FOR SERIES T (R_c 52)

Specimen	Temperature (°C)	Impact Energy (ft-lb)	Fibrosity (%)		% U _F *
			Visual	Planimeter	
T- 8	200	18.1	100	100.0	115.0
-14	160	17.8	100	100.0	107.5
-16	120	17.1	100	100.0	90.0
- 6	100	17.1	80	60.3	90.0
- 1	75	15.5	35	40.0	50.0
- 2	50	14.5	30	23.5	25.0
- 3	30	13.3	25	19.0	-
- 5	26 (R.T.)	14.5	30	22.2	25.0
-12	0	13.6	20	16.5	2.5
- 7	-40	10.0	10	10.2	-
-11	-80	8.4	5	8.1	-
-15	-120	7.0	5	1.9	-
- 4	-196	5.2	5	3.1	-
-13	-196	3.7	5	1.0	-

TABLE IV

IMPACT TEST RESULTS FOR SERIES U (R_c 52)

Specimen	Temperature (°C)	Impact Energy (ft-lb)	Fibrosity (%)	% U _F **
U-33	220	18.1	100	113.3
- 5	200	17.1	85	102.5
-19	190	17.8	100	106.7
-31	180	16.8	85	84.4
- 8	170	17.5	100	100.0
- 6	150	15.8	40	62.2
- 4	120	15.8	45	62.2
- 9	100	15.8	40	62.2
-10	80	15.2	30	48.9
-11	30	13.0	20	0
-12	0	12.7	15	-
-13	-40	10.6	10	-
-16	-80	7.8	5	-
-17	-105	8.5	5	-
-20	-130	7.3	2.5**	-
-26	-155	5.0	2.5**	-
-28	-196	4.7	2.5**	-

*For definition see appendix

**Average of two readings

TABLE V
IMPACT TEST RESULTS FOR SERIES D (R_c 47)

Specimen	Temperature (°C)	Impact Energy (ft-lb)	Fibrosity (%)	% U_F^*
D-1-470	200	19.4	100	98.2
-1-574	150	18.8	100	87.3
-2-357	100	18.8	100	87.3
-2-671	80	17.5	80	63.6
-5-771	60	18.4	60	80.0
-5-178	50	18.1	47.5**	74.5
-4-962	40	14.5	32.5**	9.1
-3-067	30	14.2	25	3.6
-3-104	0	12.7	25	-
-3-628	-40	13.6	17.5**	-
-3-712	-80	11.2	10	-
-3-786	-105	9.5	5	-
-4-276	-130	8.9	5	-
-4-294	-155	8.1	5	-
-4-310	-196	5.4	2.5**	-

TABLE VI
IMPACT TEST RESULTS FOR SERIES K (R_c 44)

Specimen	Temperature (°C)	Impact Energy (ft-lb)	Fibrosity (%)	% U_F^*
K-22	160	36.1	100	100.5
-21	140	34.5	100	92.1
-37	120	35.7	100	98.4
-35	100	37.7	100	108.9
-17	90	34.5	85	92.1
-31	80	31.4	70	75.8
-14	70	31.4	70	75.8
- 9	60	30.2	65	69.5
- 6	50	23.3	40	33.2
- 5	40	20.8	30	20.0
-10	30	20.1	17.5**	16.3
-11	0	19.1	12.5**	11.0
-12	-40	9.5	5	-
-13	-80	11.2	5	-
-15	-105	8.4	2.5**	-
-19	-130	6.7	0	-
-20	-155	4.2	0	-
-26	-196	4.4	0	-

*For definition see appendix

**Average of two readings

TABLE VII

IMPACT TEST RESULTS FOR SERIES S (R_c 42)

Specimen	Temperature (°C)	Impact Energy (ft-lb)	Fibrosity (%)		% U_F *
			Visual	Planimeter	
S- 5	26	31.4	100	100.0	114.5
-11	0	29.8	100	100.0	104.8
-13	-20	29.8	100	100.0	104.8
- 1	-30	25.8	80	69.2	80.6
- 6	-40	24.3	80	67.5	71.5
- 2	-50	21.1	65	54.0	52.1
-12	-60	18.4	40	37.4	35.8
- 7	-80	15.2	25	17.7	16.4
- 4	-100	14.2	15	13.8	10.3
- 8	-120	14.2	15	8.6	10.3
- 9	-155	13.9	10	8.0	8.5
-14	-155	12.1	10	8.8	-
-10	-196	10.5	5	5.5	-

TABLE VIII

IMPACT TEST RESULTS FOR SERIES E (R_c 37)

Specimen	Temperature (°C)	Impact Energy (ft-lb)	Fibrosity (%)	% U_F *
E-1-018	80	43.6	100	115.9
-1-351	30	46.6	100	126.2
-2-055	0	47.0	100	127.6
-2-427	-40	46.6	100	126.2
-5-156	-60	46.1	100	124.5
-1-524	-70	37.7	95	95.5
-2-638	-80	29.8	85	68.3
-5-242	-90	29.8	70	68.3
-2-704	-100	17.8	25	26.9
-3-351	-105	18.4	30	28.9
-3-406	-130	18.4	25	28.9
-1-820	-155	14.5	17.5**	15.5
-4-928	-196	11.5	10	5.2

*For definition see appendix

**Average of two readings

TABLE IX

IMPACT TEST RESULTS FOR SERIES J (R_c 36)

Specimen	Temperature (°C)	Impact Energy (ft-lb)	Fibrosity (%)	% U _F *
J-14	140	56.7	100	118.9
-37	120	55.4	100	115.2
-13	100	51.3	100	103.4
- 5	80	50.1	97.5**	100.3
-10	70	47.0	85	91.5
- 9	60	26.2	40	33.0
- 8	50	25.4	30	30.7
- 6	40	25.4	25	30.7
- 7	30	18.1	15	10.1
-34	20	18.1	10	10.1
-12	0	13.6	5	-
-17	-40	12.4	2.5**	-
-19	-80	8.1	0	-
-25	-105	5.2	0	-
-30	-130	6.0	0	-
-32	-155	5.2	0	-
-33	-196	3.2	0	-

TABLE X

IMPACT TEST RESULTS FOR SERIES P (R_c 33)

Specimen	Temperature (°C)	Impact Energy (ft-lb)	Fibrosity (%)		% U _F *
			Visual	Planimeter	
P- 5	26	66.5	100	100.0	128.4
-16	0	65.1	100	100.0	125.2
-15	-20	64.6	100	100.0	124.1
- 6	-40	62.2	100	100.0	118.6
-14	-60	60.4	100	100.0	114.5
- 7	-80	59.1	100	100.0	111.6
-13	-90	58.6	100	100.0	110.4
-11	-100	48.3	90	85.0	87.0
-12	-110	54.9	100	100.0	102.0
- 8	-120	33.7	75	58.0	53.9
- 3	-130	35.3	75	63.2	57.5
- 2	-140	23.9	40	34.9	31.6
- 4	-155	19.7	20	21.2	22.0
- 9	-155	20.5	20	19.0	23.9
-10	-196	17.5	10	9.1	17.0

*For definition see appendix

**Average of two readings

TABLE XI
IMPACT TEST RESULTS FOR SERIES F (R_c 28)

Specimen	Temperature (°C)	Impact energy (ft-lb)	% Fibrosity	% U _F *
F- 953	24	81.0	100	148.4
-1-827	0	76.0	100	138.1
-4-709	-20	76.0	100	138.1
-1-737	-40	79.9	100	146.2
- 329	-40	75.0	100	136.1
-5-117	-60	76.5	100	139.2
-1-720	-80	72.7	100	131.3
-2-469	-80	68.5	100	122.7
- 308	-80	66.0	100	117.5
- 975	-90	56.5	85	97.9
-5-010	-90	57.5	100	100.0
-2-959	-100	46.5	80	77.3
- 544	-100	49.5	85	83.5
-4-040	-105	35.7	55	55.0
-6-343	-110	31.0	55	45.4
-1-018	-110	33.5	55	50.5
-4-963	-120	23.3	35	29.5
-4-142	-130	31.0	50	45.4
-8-111	-140	22.2	25	27.2
-4-500	-155	23.9	30	30.7
-4-521	-196	16.8	15	16.1

TABLE XII
IMPACT TEST RESULTS FOR SERIES O (R_c 15)

Specimen	Temperature (°C)	Impact Energy (ft-lb)	Fibrosity (%)		% U _F *
			Visual	Planimeter	
0- 2	120	58.2	100	100.0	101.4
- 6	100	59.1	100	100.0	103.2
- 1	80	59.1	100	100.0	103.2
- 8	60	59.6	100	100.0	104.2
-12	50	53.6	95	91.0	92.2
-10	40	43.2	85	72.9	71.4
- 3	30	43.2	75	68.9	71.4
- 5	26	25.4	45	39.0	35.8
0-11	0	20.8	25	20.6	26.6
- 7	-40	13.0	10	7.8	11.0
-15	-60	18.4	5	9.1	21.8
- 9	-80	8.4	0	1.2	-
-14	-100	5.4	0	0.8	-
- 4	-120	3.4	0	0	-
-13	-155	2.1	0	0	-
-16	-196	1.5	0	0	-

*For definition see appendix

TABLE XIII
IMPACT TEST RESULTS FOR SERIES N (R_c 12)

Specimen	Temperature (°C)	Impact Energy (ft-lb)	Fibrosity (%)		% U_F *
			Visual	Planimeter	
N- 3	120	58.6	100	100.0	101.1
- 6	100	63.7	100	100.0	110.8
- 2	80	53.1	100	100.0	90.8
- 8	60	64.1	100	100.0	111.5
-12	50	42.3	85	69.3	70.4
-10	40	31.8	65	52.0	50.6
- 5	26	25.4	40	36.9	38.5
-11	0	18.4	20	21.9	25.3
- 7	-40	15.5	5	6.9	19.8
-13	-40	7.5	5	6.2	4.7
- 9	-80	4.2	0	0	-
- 4	-100	3.0	0	1.8	-
-14	-120	1.8	0	0	-
-15	-155	1.5	0	0	-
-16	-196	1.3	0	0	-

TABLE XIV
IMPACT TEST RESULTS FOR SERIES M (R_c 12)

Specimen	Temperature (°C)	Impact Energy (ft-lb)	Fibrosity (%)	% U_F *
M- 1	200	64.6	100	109.6
- 2	150	70.8	100	121.3
- 3	100	60.0	100	100.9
- 4	80	58.6	100	98.3
-36	70	44.4	62.5**	71.5
-29	60	41.9	67.5**	66.8
-26	50	39.8	57.5**	62.8
- 5	30	21.5	27.5**	28.3
- 7	0	17.5	22.5**	20.8
-11	-40	7.8	5	2.4
-12	-80	4.4	0	-
-13	-105	2.5	0	-
-19	-130	1.8	0	-
-22	-155	2.3	0	-
-25	-196	2.8	0	-

*For definition see appendix

**Average of two readings

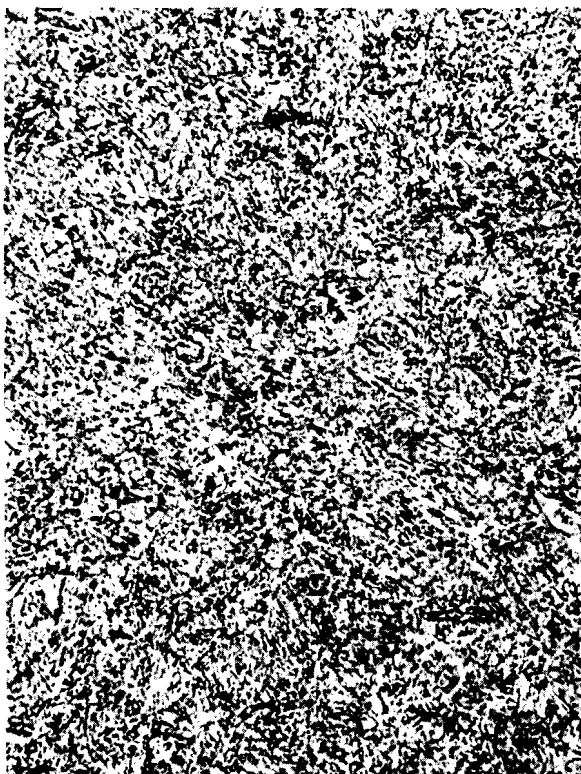
TABLE XV

SUMMARY OF RESULTS

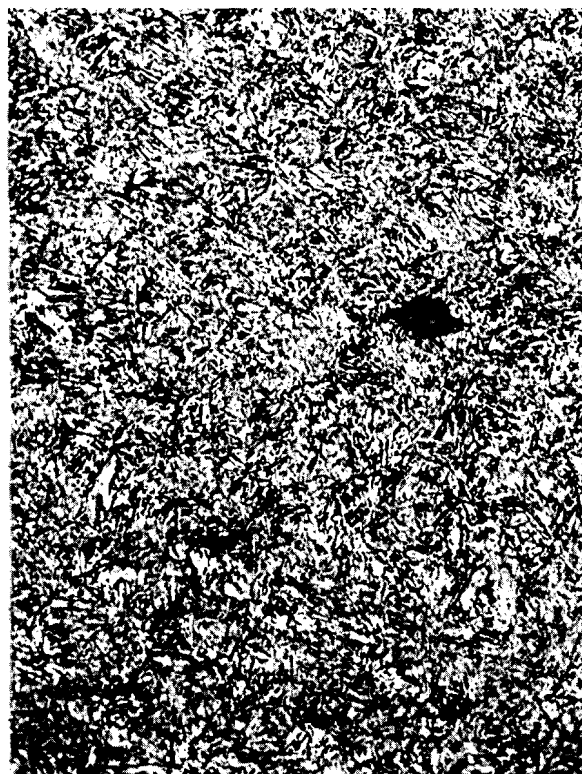
Series	Impact Energy (ft-lb)			Transition Temp. (°C)			M (ft-lb/°C)	n	Total Elong. ** (%)
	U ₁₀₀ *	U ₀ *	U _F	TT ₁₀₀	TT ₀	ΔTT			
T	17.5	13.5	4.0	120	20	100	0.04	0.038	14
U	17.5	13.0	4.5	205	30	175	0.03	0.039	12
D	19.5	14.0	5.5	100	0	100	0.06	0.044	12
K	36.0	17.0	19.0	100	20	80	0.24	0.067	17
S	29.0	12.5	16.5	-20	-85	65	0.25	0.059	15
E	39.0	10.0	29.0	-70	-120	50	0.58	0.073	19
J	50.0	14.5	35.5	85	30	55	0.64	0.071	17
P	54.0	10.0	44.0	-100	-150	50	0.88	0.100	21
F	57.5	9.0	48.5	-90	-140	50	0.97	0.125	27
O	57.5	7.5	50.0	60	0	60	0.83	0.140	25
N	58.0	5.0	53.0	70	-10	80	0.66	0.136	29
M	59.5	6.5	53.0	80	0	80	0.66	0.130	29

*Intercept from impact energy-fibrosity graph (Figures 22-25).

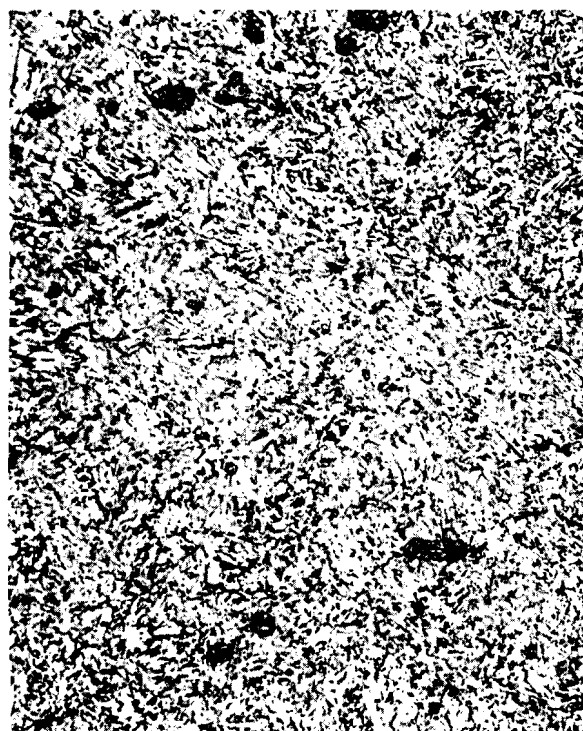
**1" gage length.



T

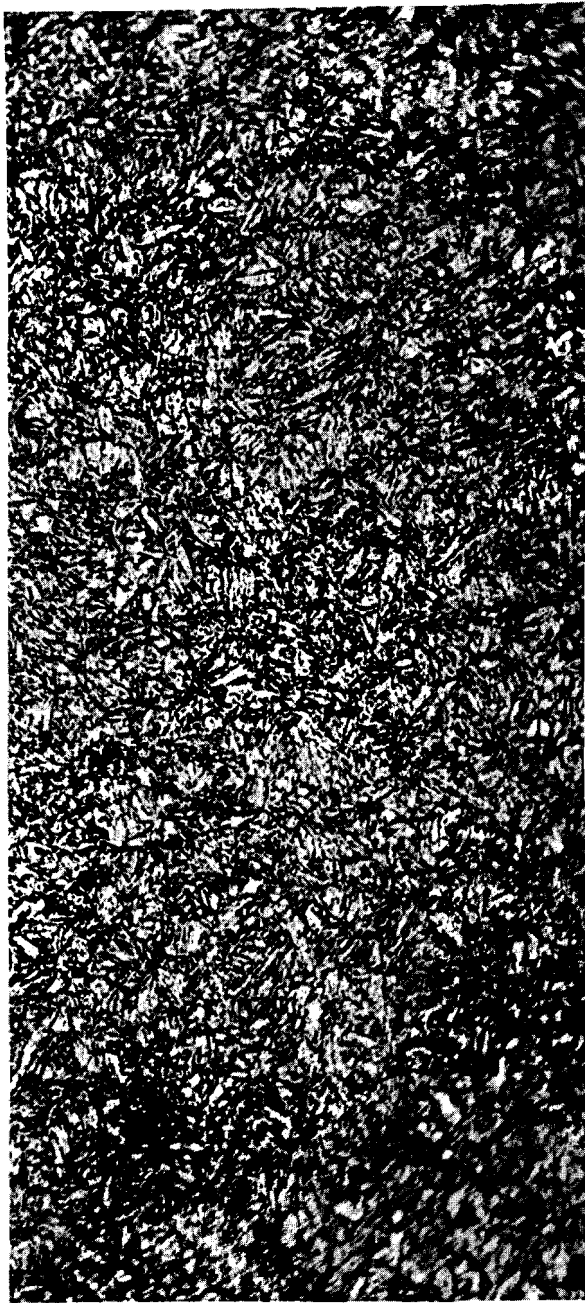


U



D

SERIES T, U AND D - TYPICAL MARTENSITIC MICROSTRUCTURES
AT 1000X MAGNIFICATION

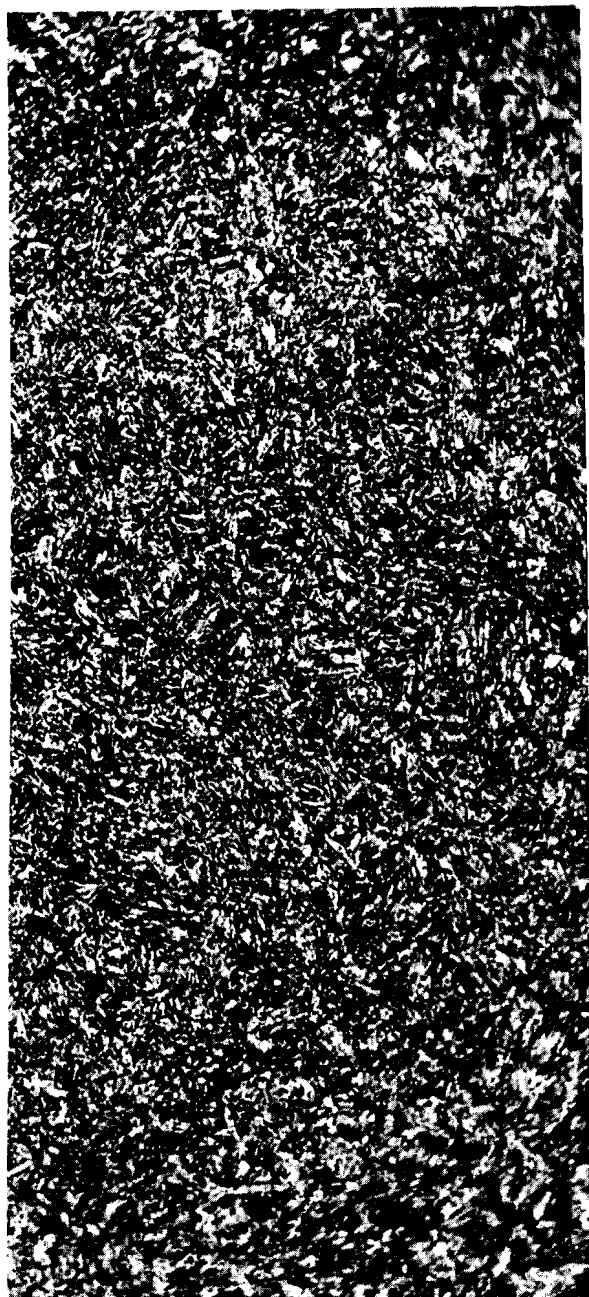


S

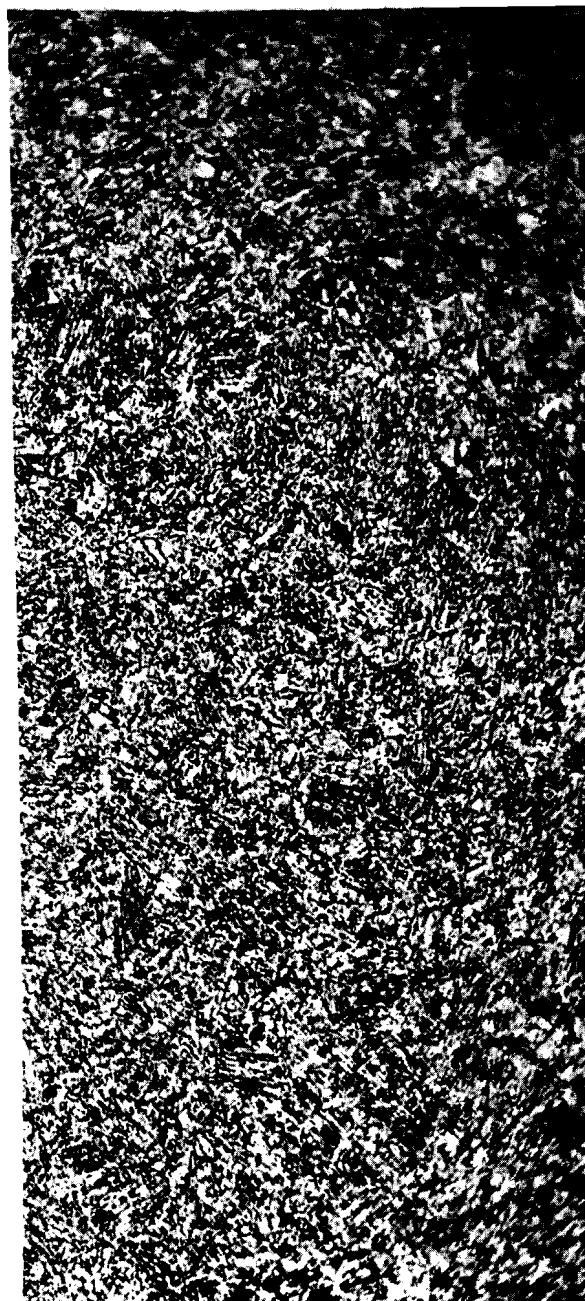


E

SERIES S AND E - TYPICAL MARTENSITIC MICROSTRUCTURES AT 1000X MAGNIFICATION

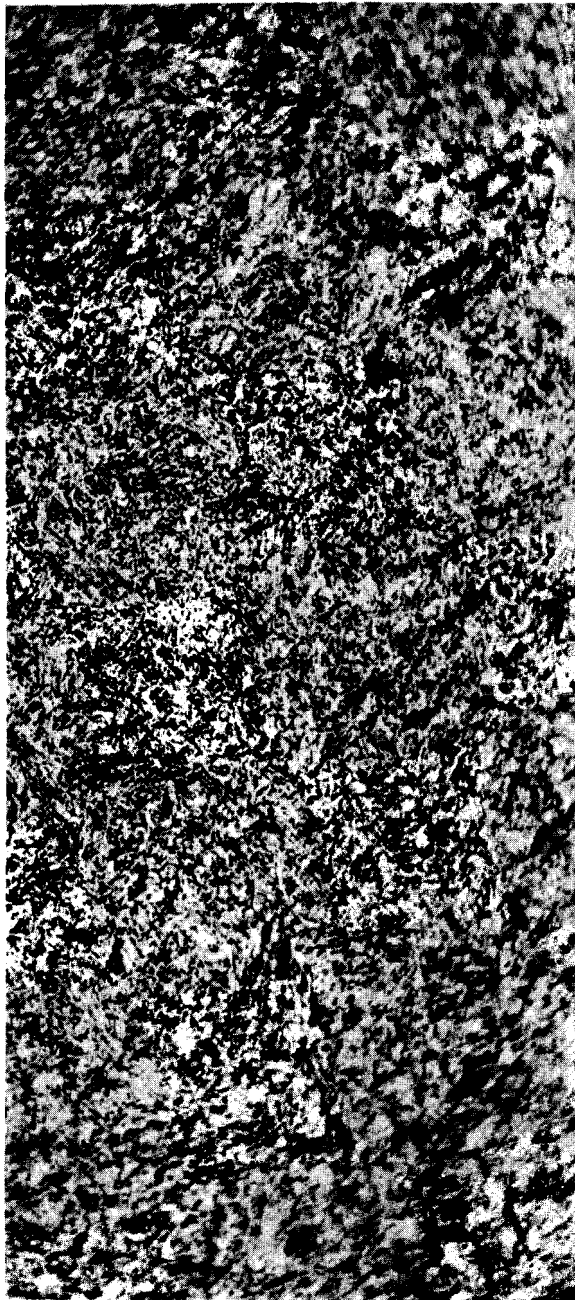


P

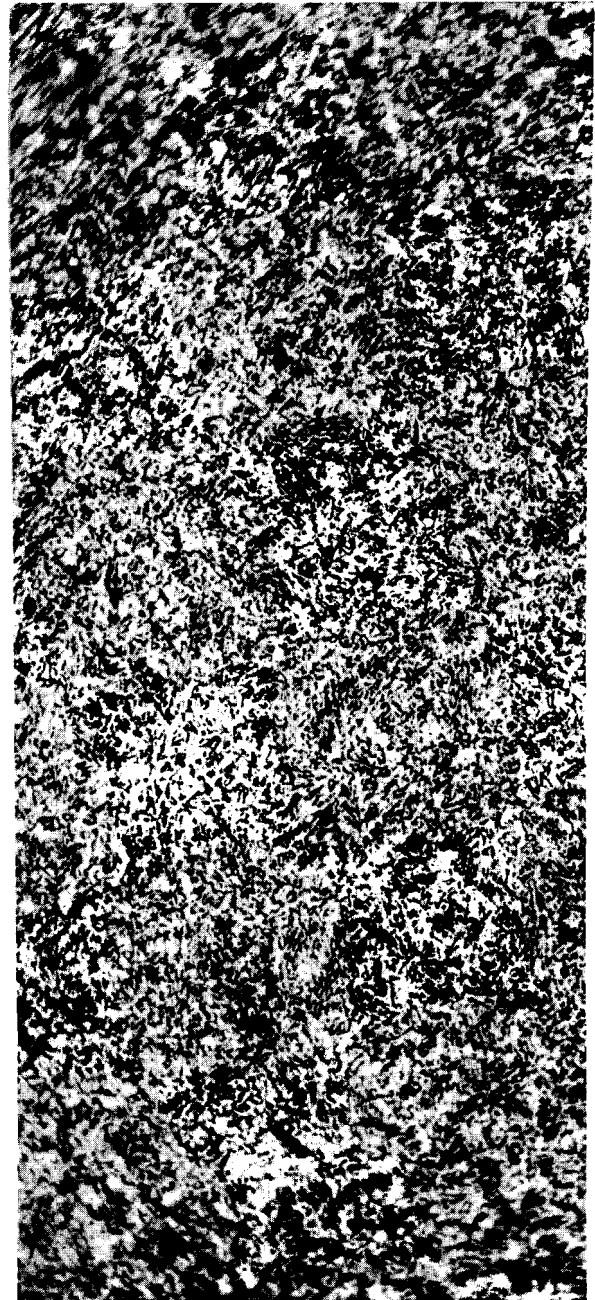


F

SERIES P AND F - TYPICAL MARTENSITIC MICROSTRUCTURES AT 1000X MAGNIFICATION



K

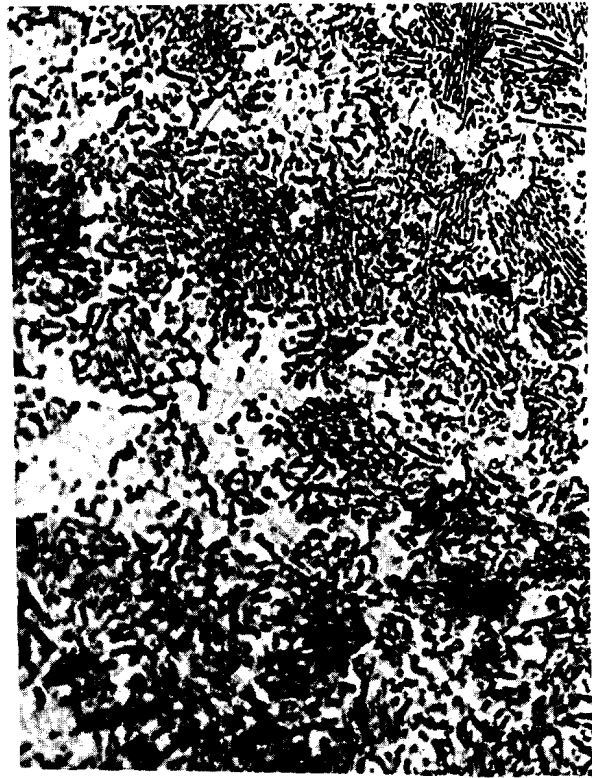


J

SERIES K AND J - TYPICAL BAINITIC MICROSTRUCTURES AT 1000X MAGNIFICATION



O



N

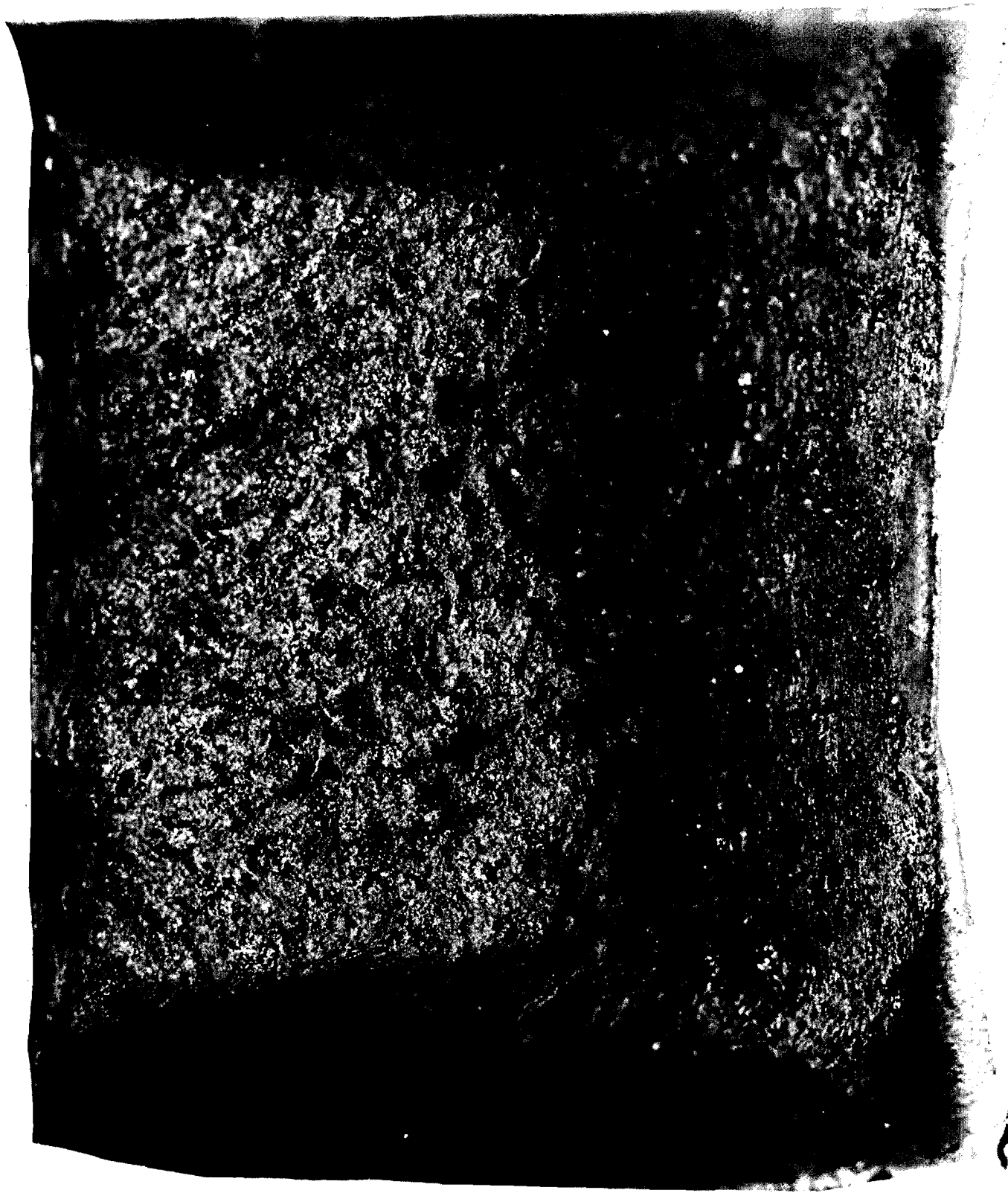


M

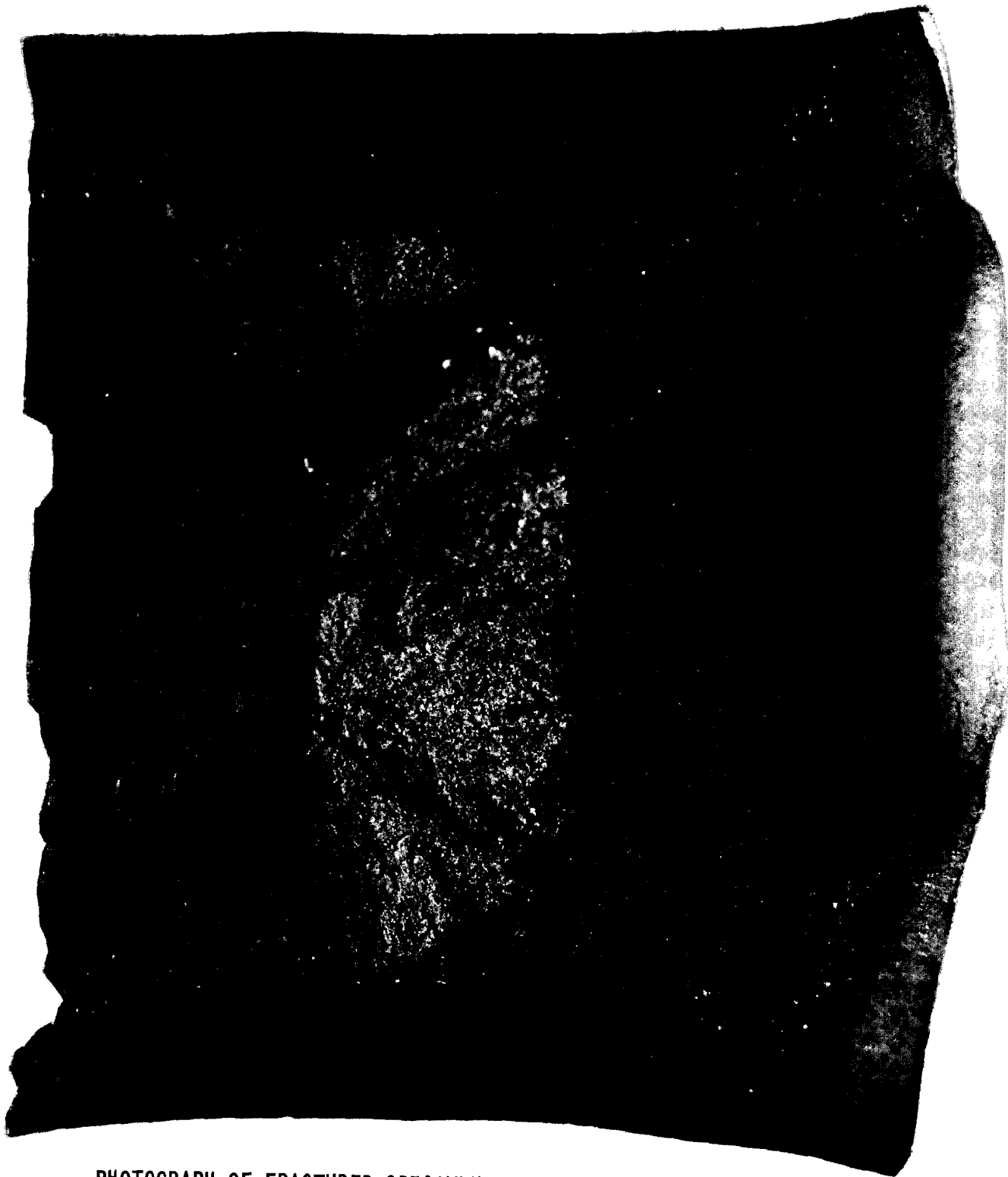
SERIES O, N AND M - TYPICAL PEARLITIC MICROSTRUCTURES
AT 1000X MAGNIFICATION



PHOTOGRAPH OF FRACTURED SPECIMEN SURFACE, P-3, AT 20X MAGNIFICATION



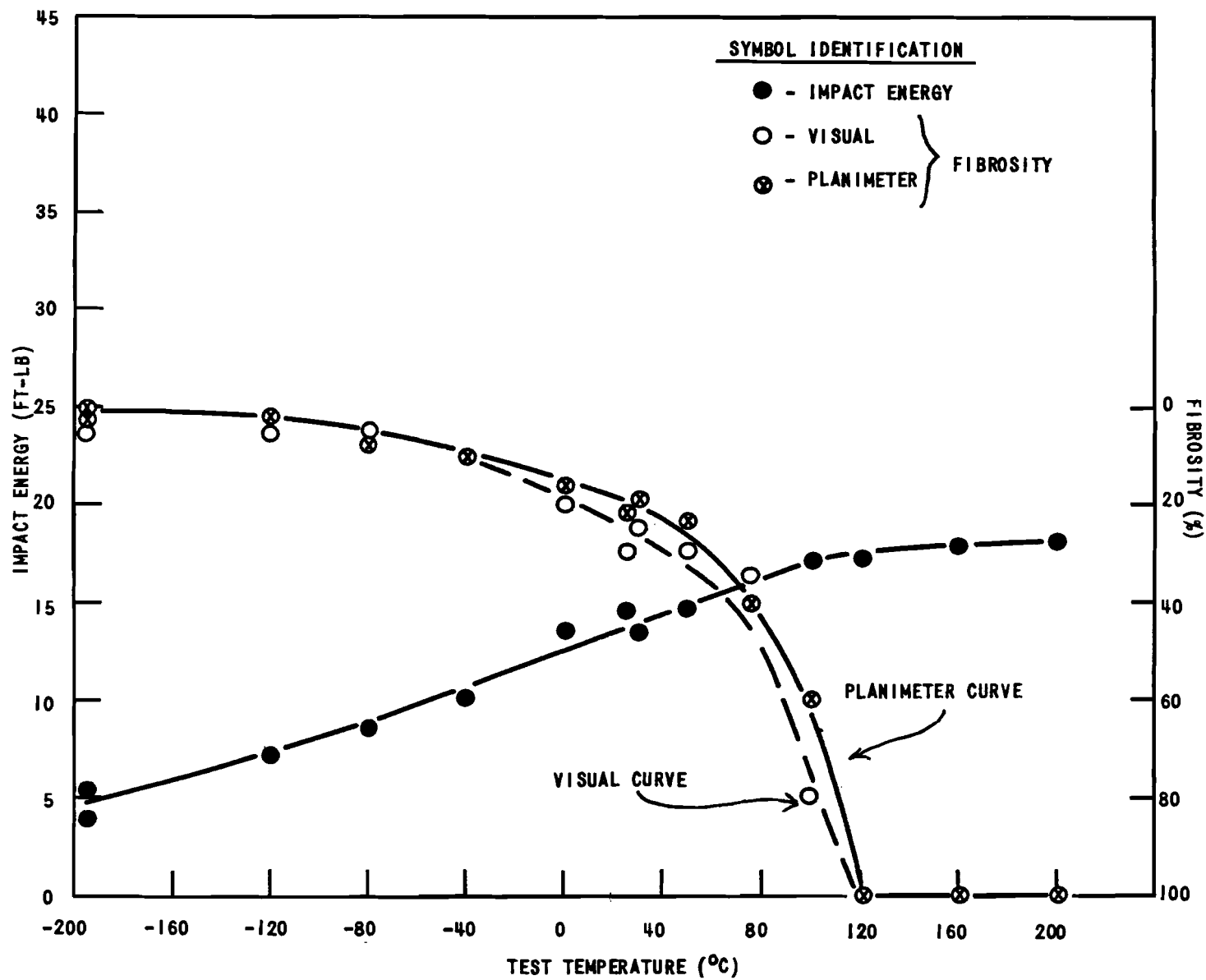
PHOTOGRAPH OF FRACTURED SPECIMEN SURFACE, S-2, AT 20X MAGNIFICATION



PHOTOGRAPH OF FRACTURED SPECIMEN SURFACE, P-11, AT 20X MAGNIFICATION



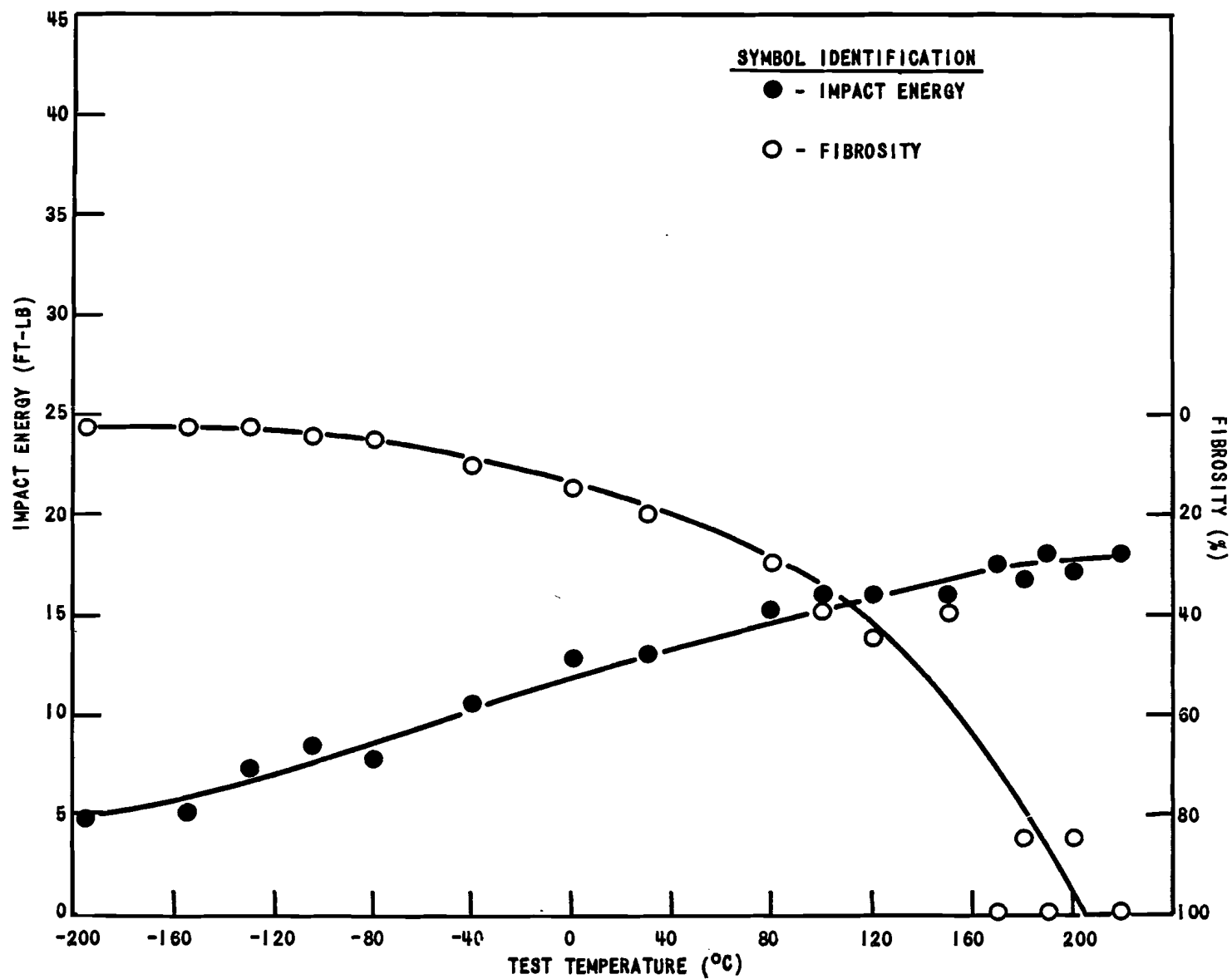
PHOTOGRAPH OF FRACTURED SPECIMEN SURFACE, 0-10, AT 20X MAGNIFICATION



IMPACT ENERGY AND FIBROSITY VERSUS TESTING TEMPERATURE - SERIES T

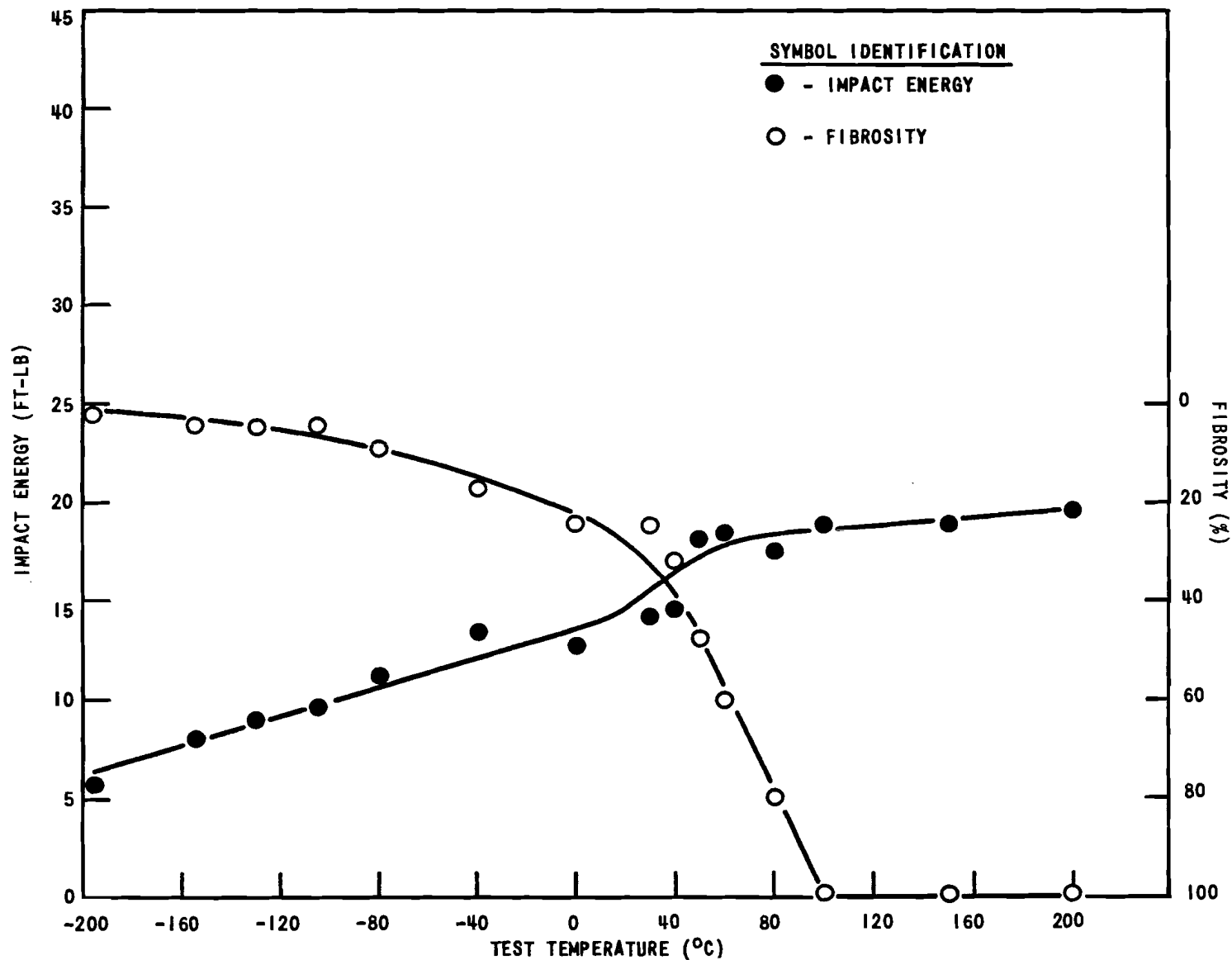
FIGURE 10

FIGURE 11



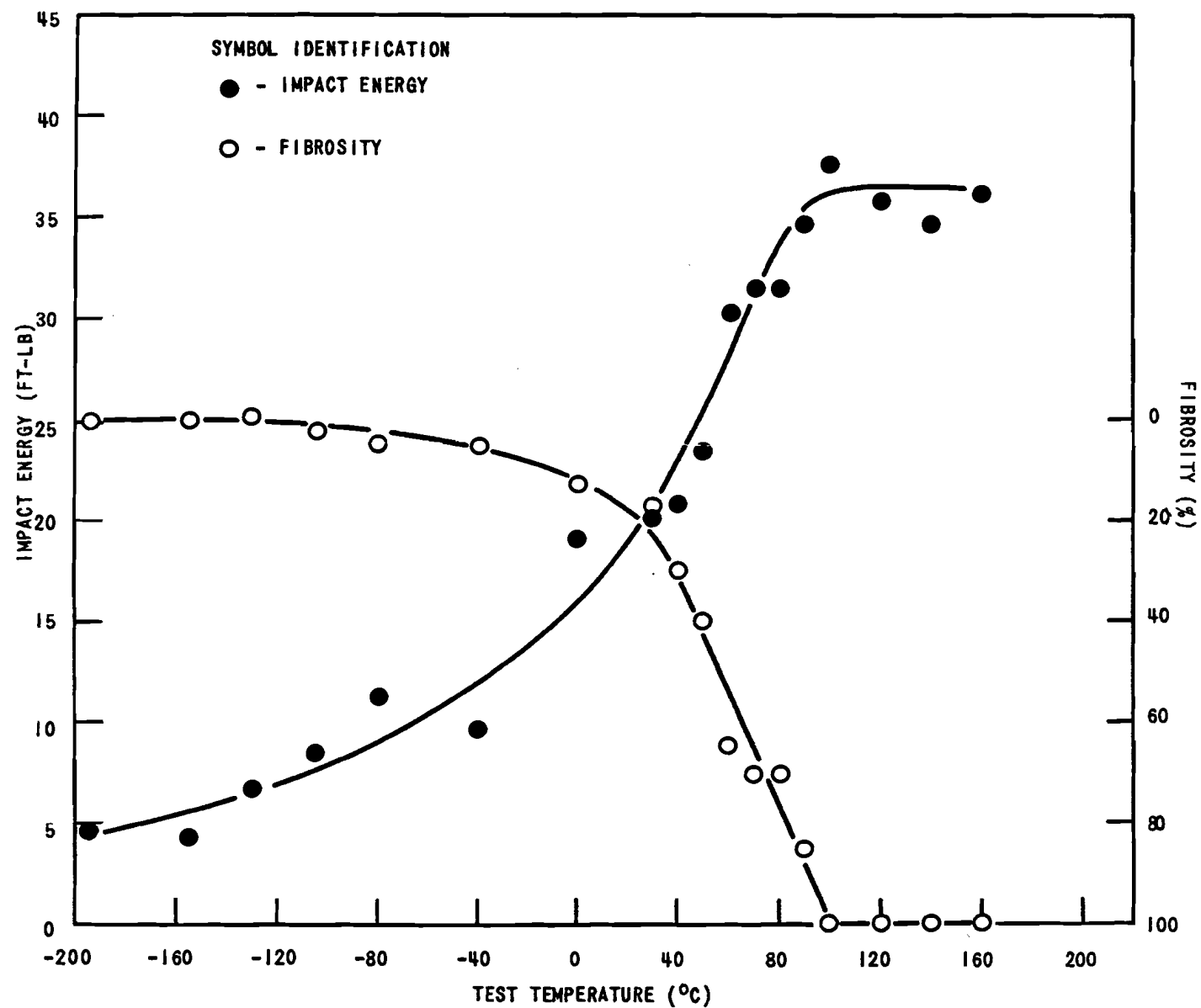
IMPACT ENERGY AND FIBROSITY VERSUS TESTING TEMPERATURE - SERIES U

FIGURE 12

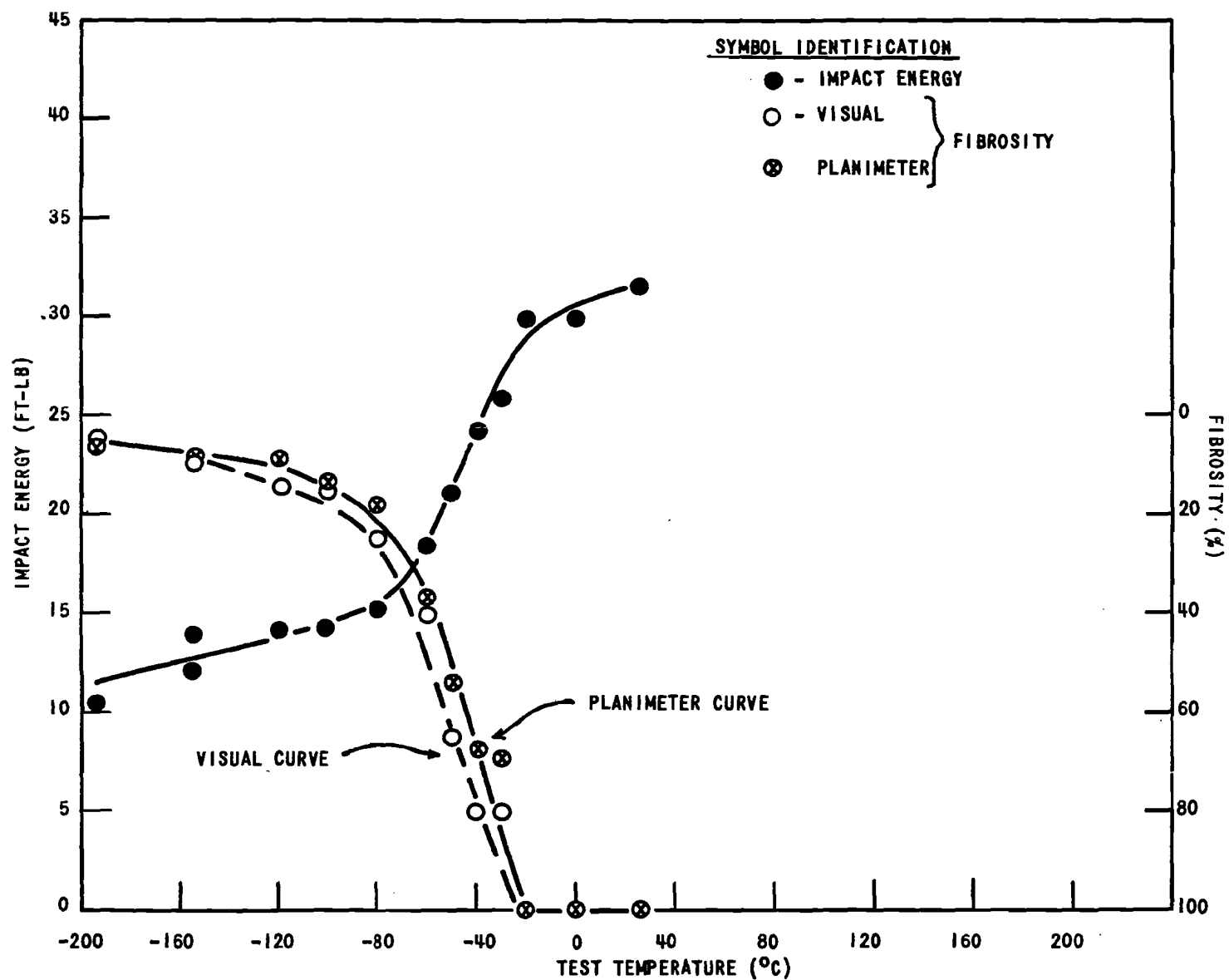


IMPACT ENERGY AND FIBROSITY VERSUS TESTING TEMPERATURE - SERIES D

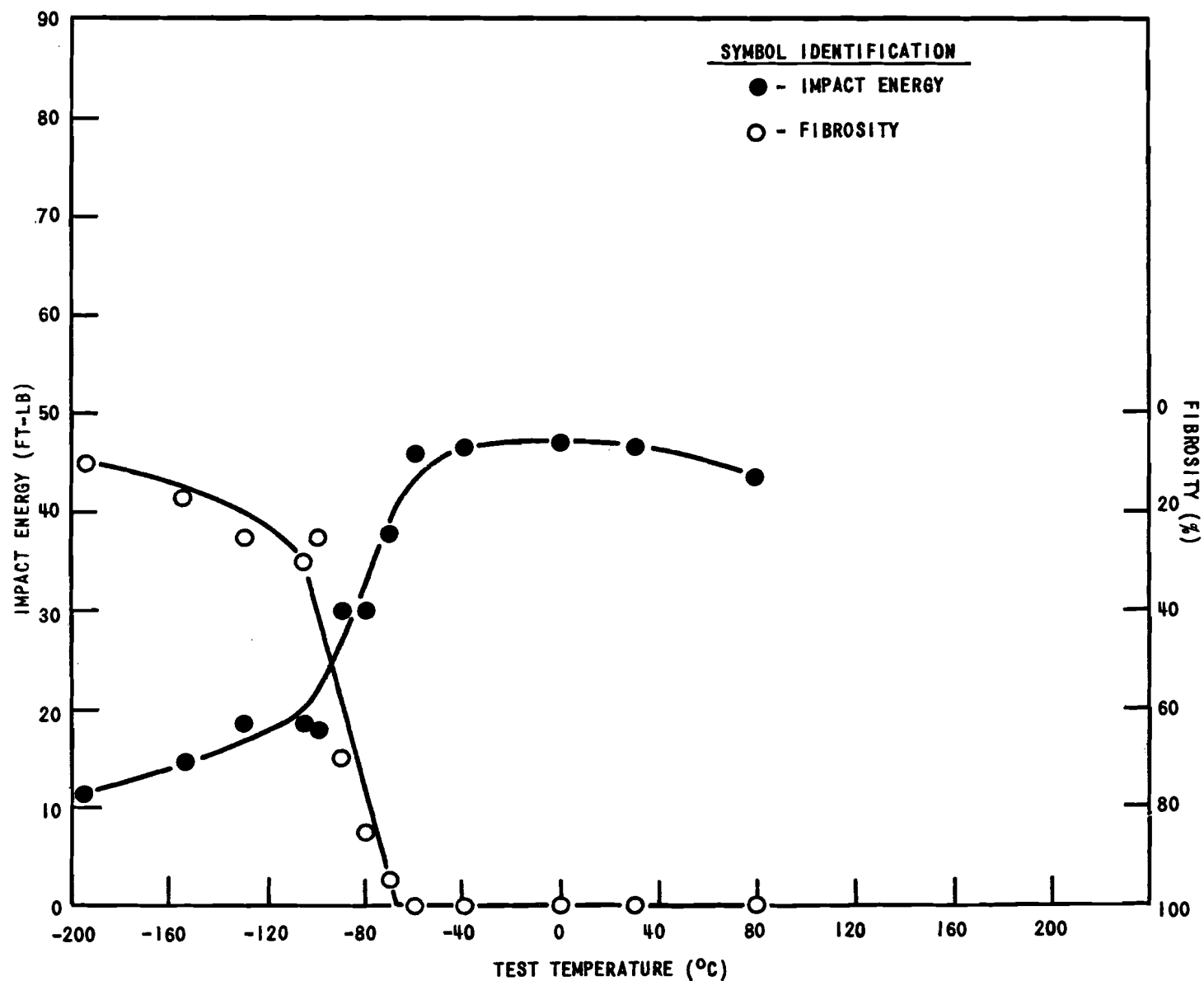
FIGURE 13



IMPACT ENERGY AND FIBROSITY VERSUS TESTING TEMPERATURE - SERIES K



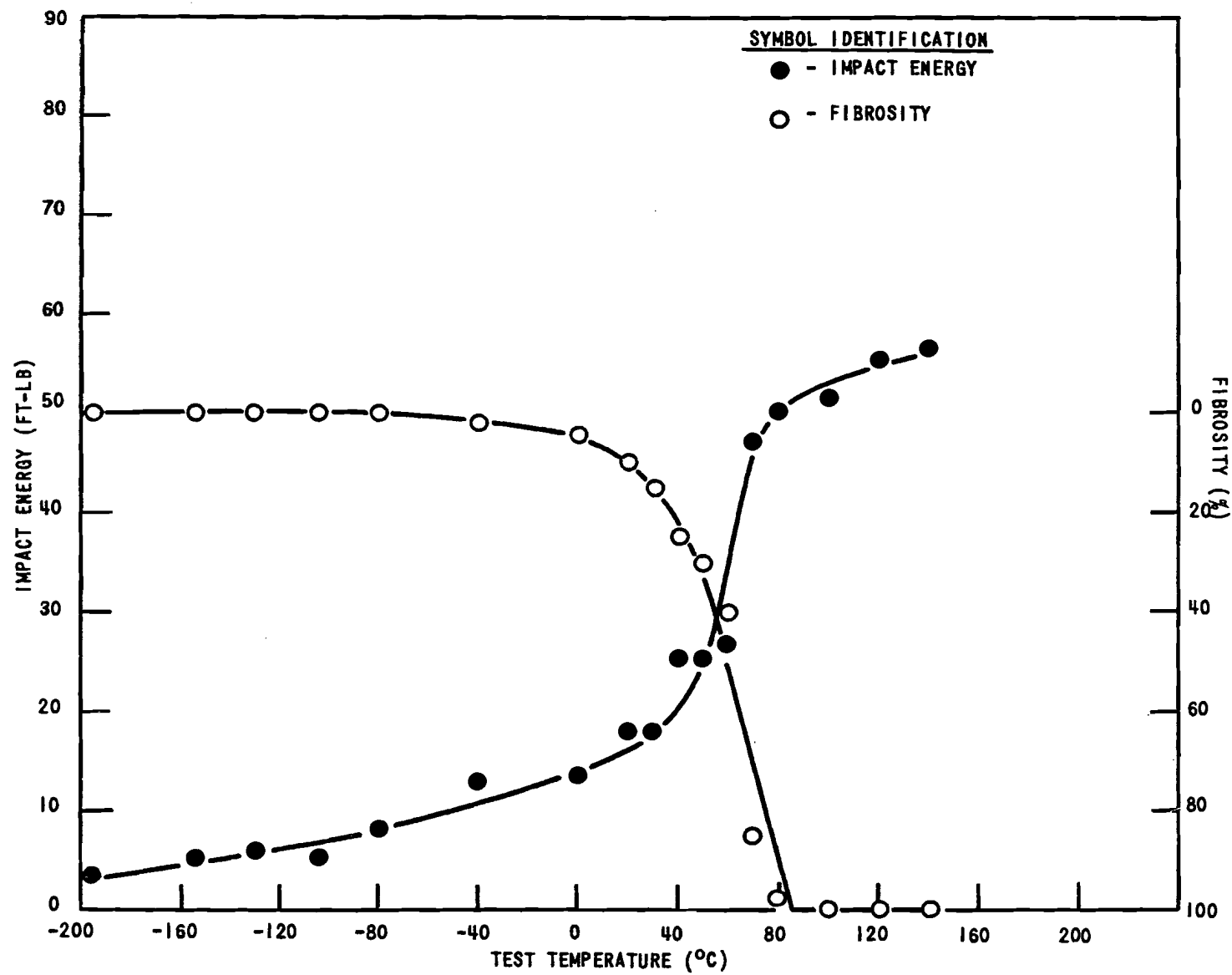
IMPACT ENERGY AND FIBROSITY VERSUS TESTING TEMPERATURE - SERIES S



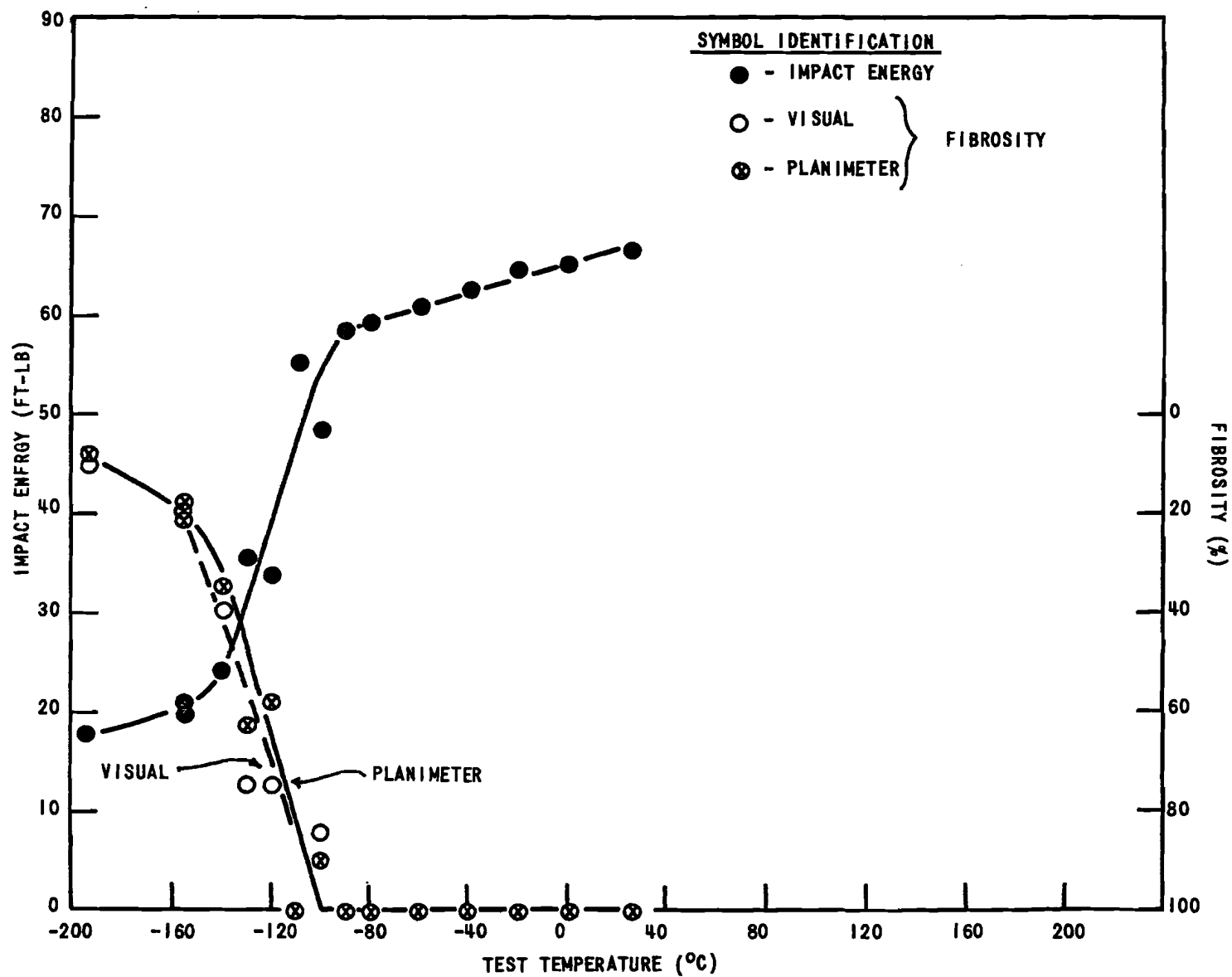
IMPACT ENERGY AND FIBROSITY VERSUS TESTING TEMPERATURE - SERIES E

FIGURE 15

FIGURE 16



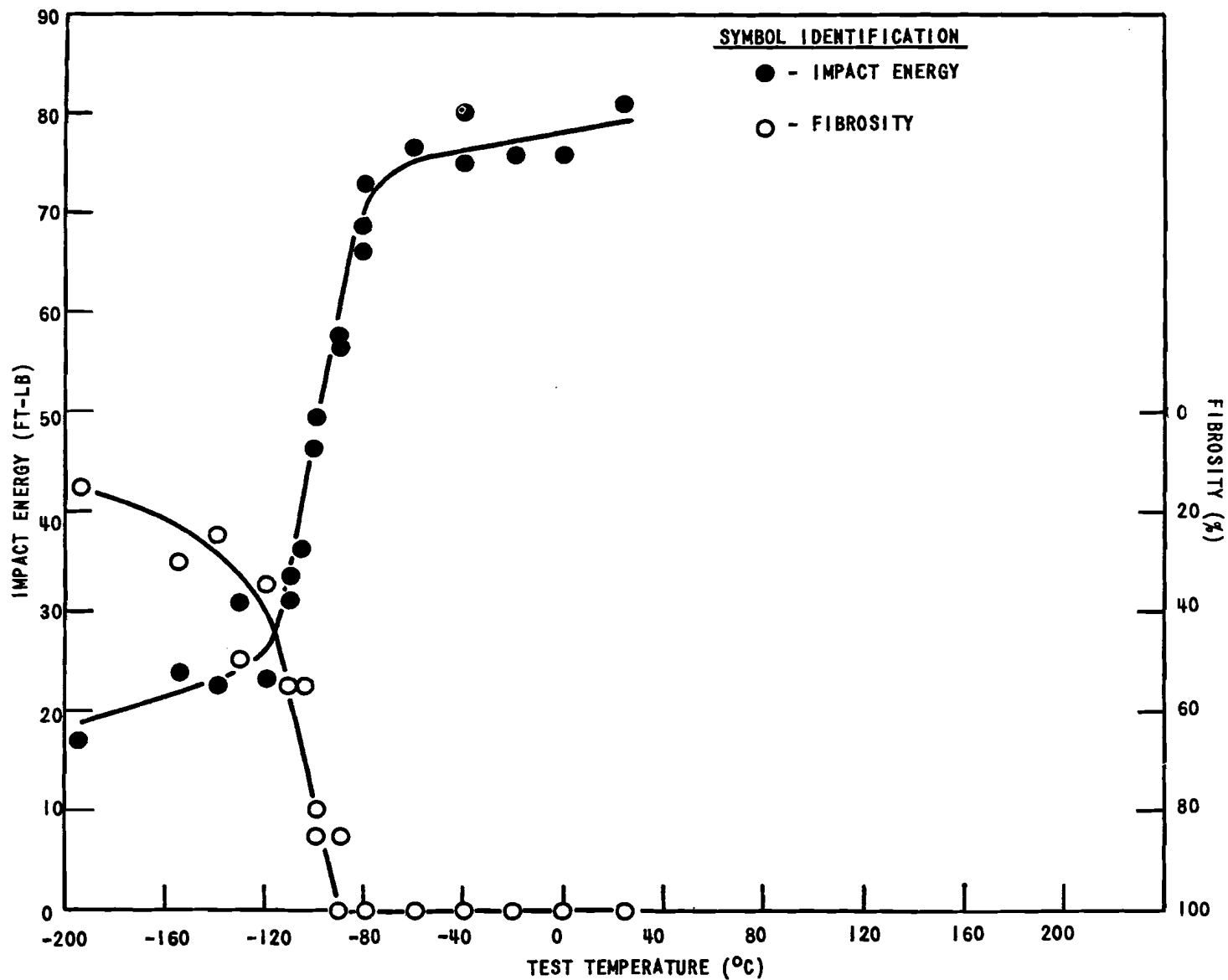
IMPACT ENERGY AND FIBROSITY VERSUS TESTING TEMPERATURE - SERIES J



IMPACT ENERGY AND FIBROSITY VERSUS TESTING TEMPERATURE - SERIES P

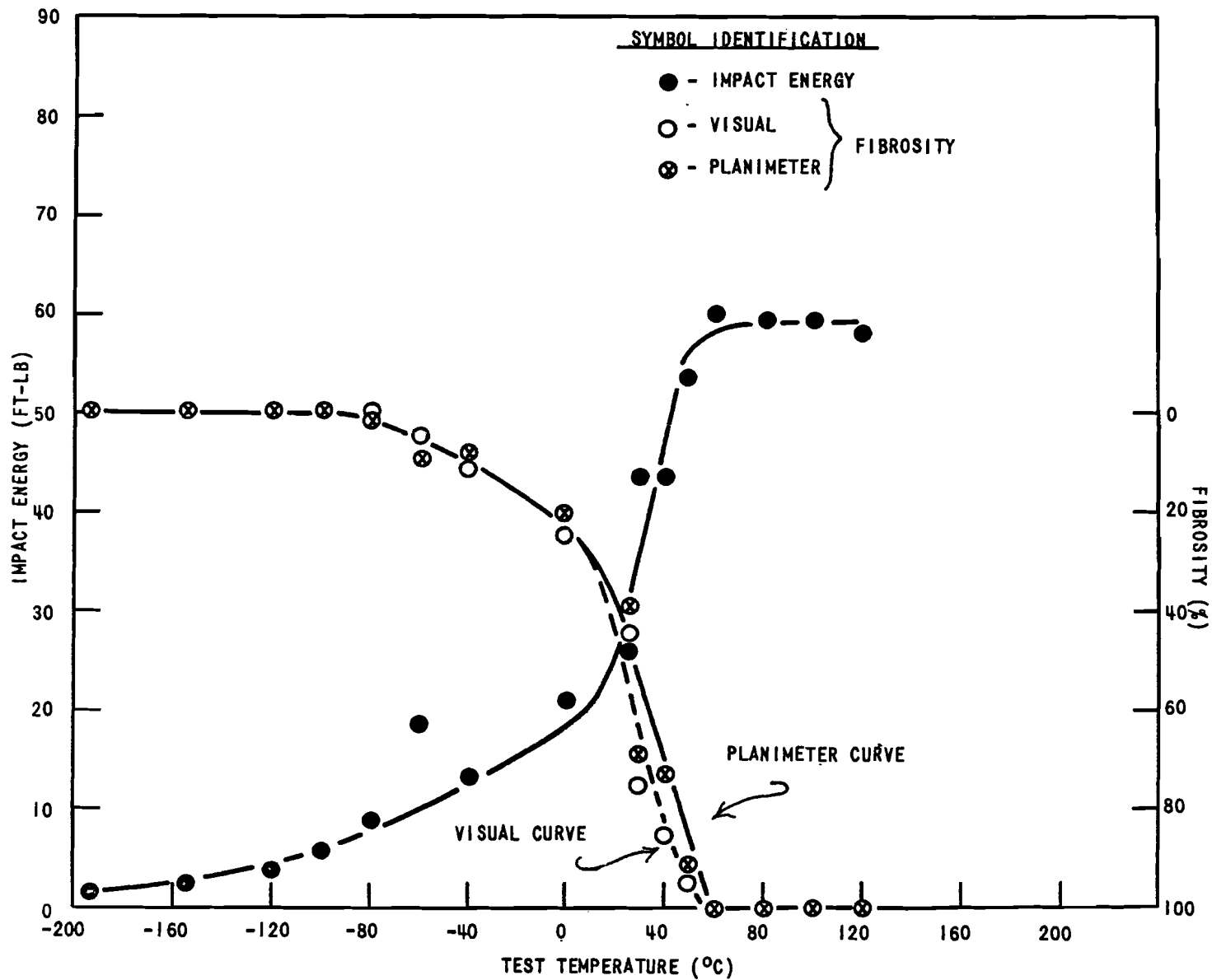
FIGURE 17

FIGURE 18



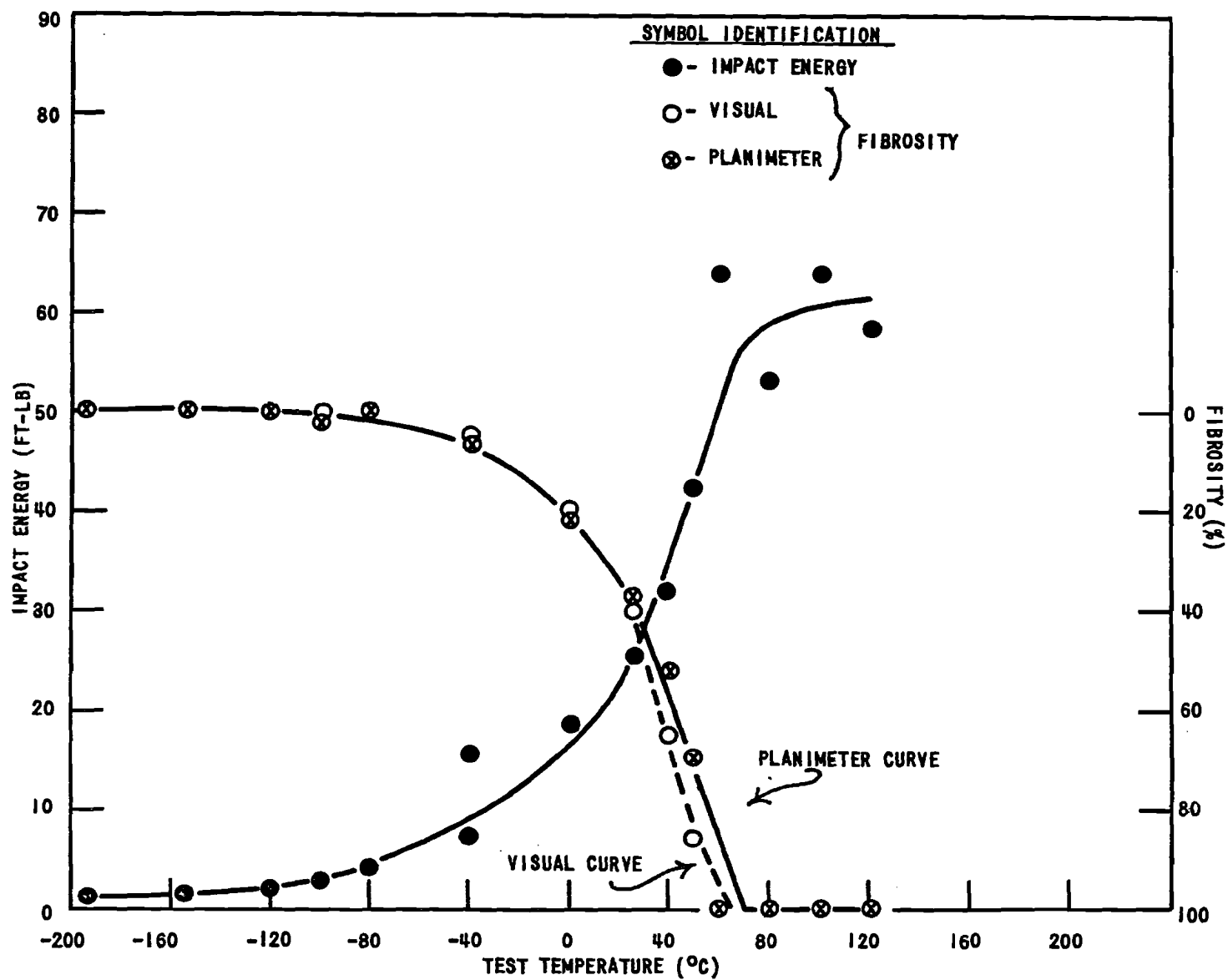
IMPACT ENERGY AND FIBROSITY VERSUS TESTING TEMPERATURE - SERIES F

FIGURE 19



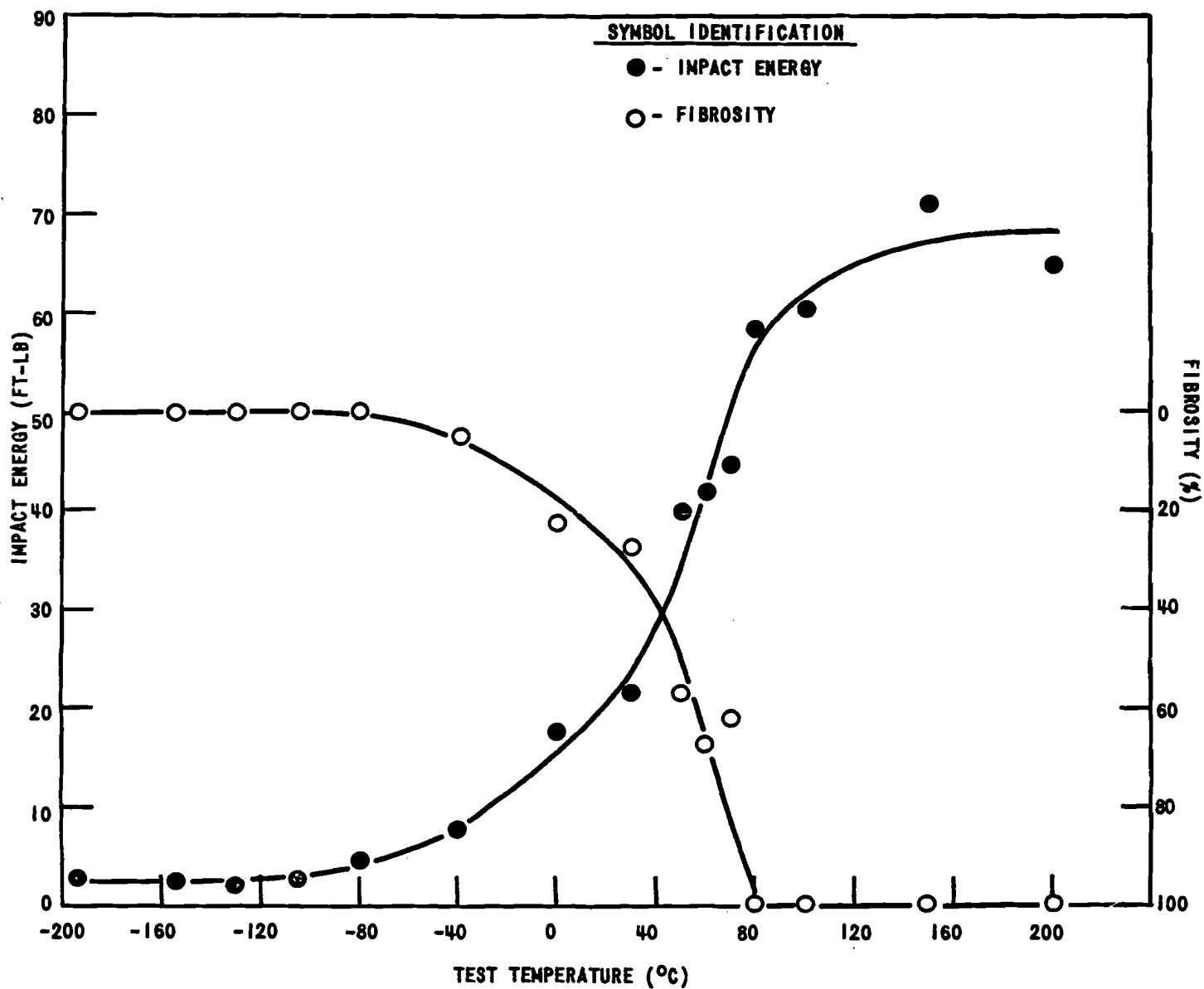
IMPACT ENERGY AND FIBROSITY VERSUS TESTING TEMPERATURE - SERIES 0

FIGURE 20



IMPACT ENERGY AND FIBROSITY VERSUS TESTING TEMPERATURE - SERIES N

FIGURE 21



IMPACT ENERGY AND FIBROSITY VERSUS TESTING TEMPERATURE - SERIES M

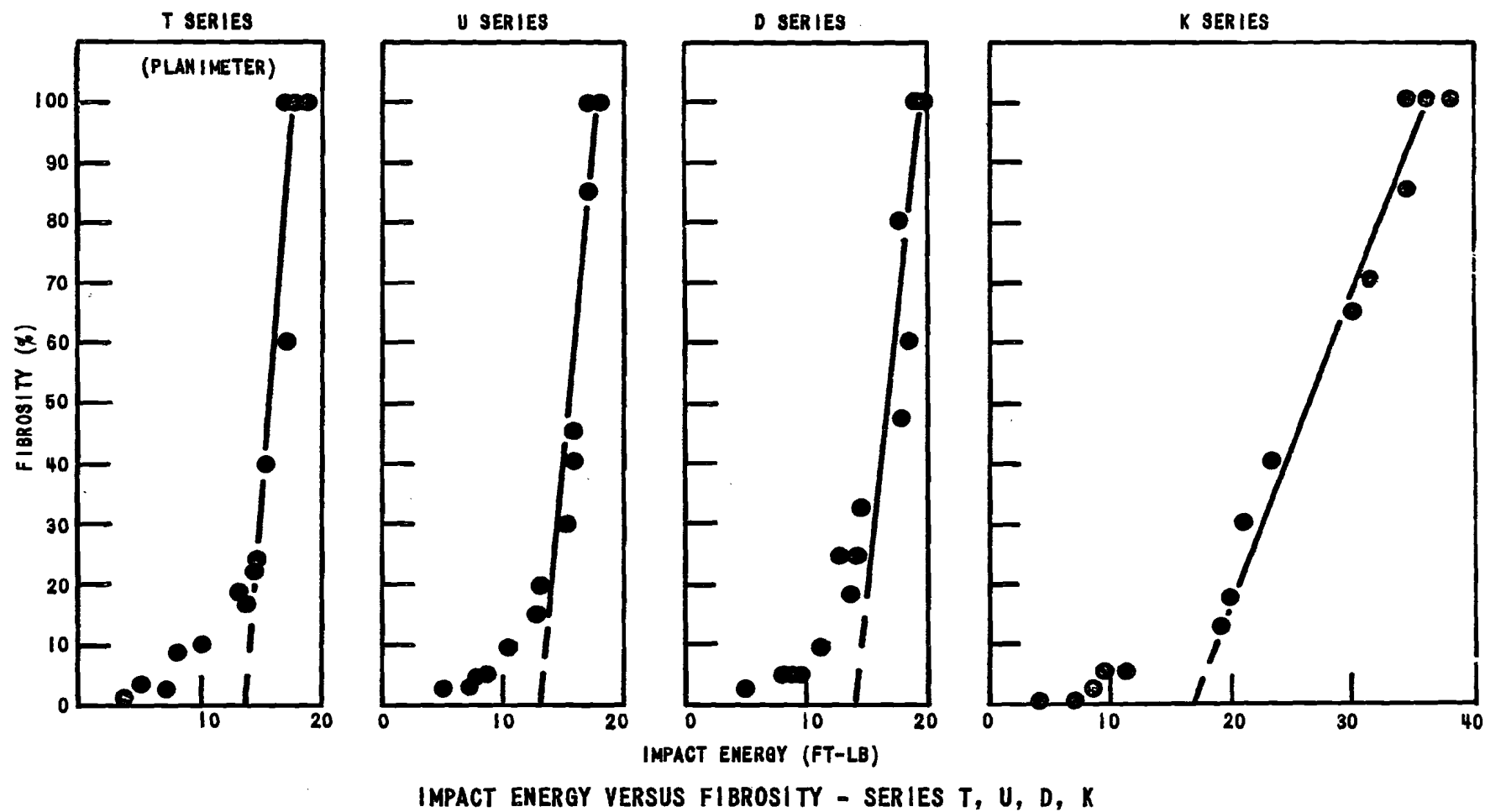
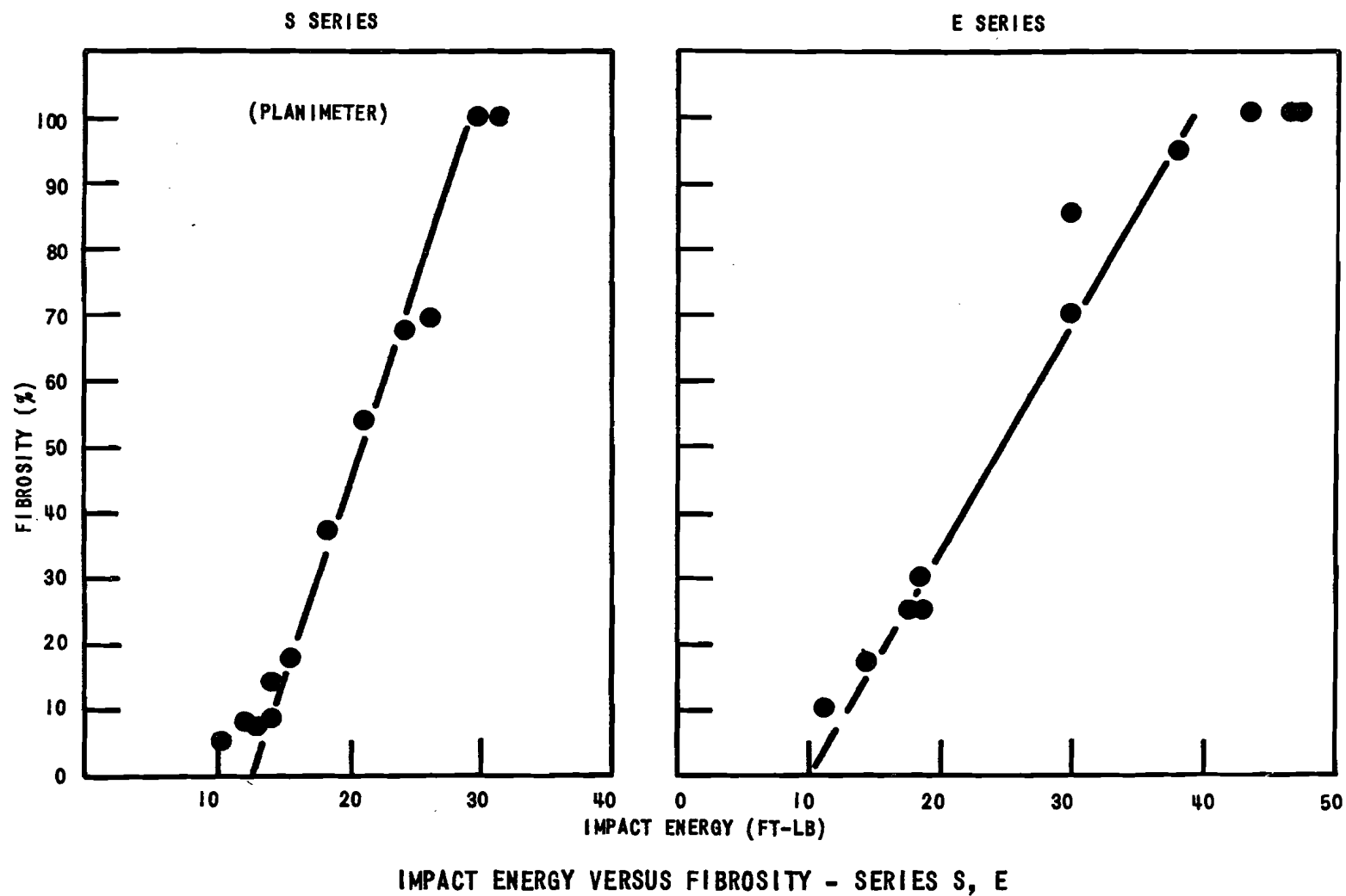


FIGURE 23



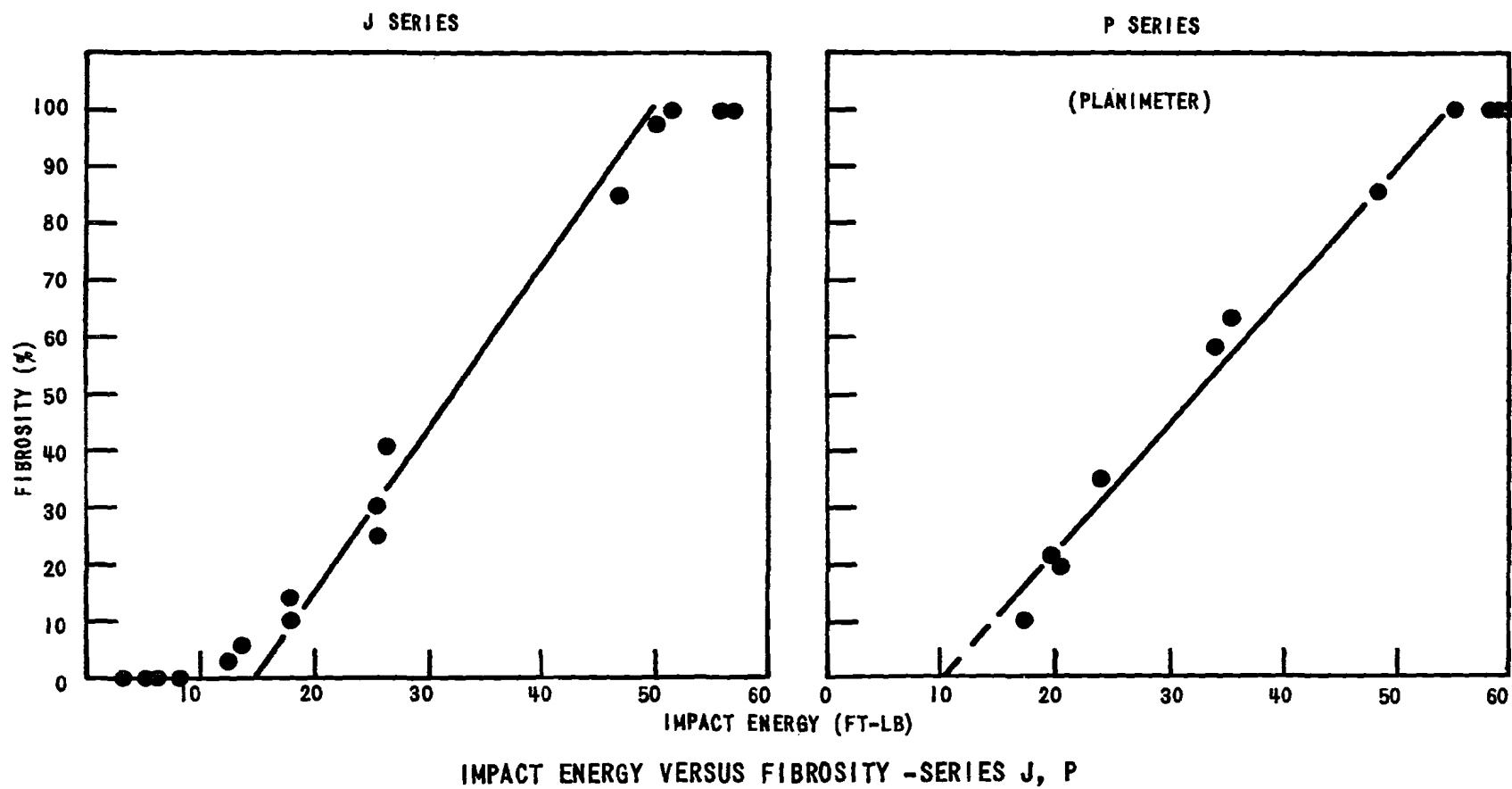
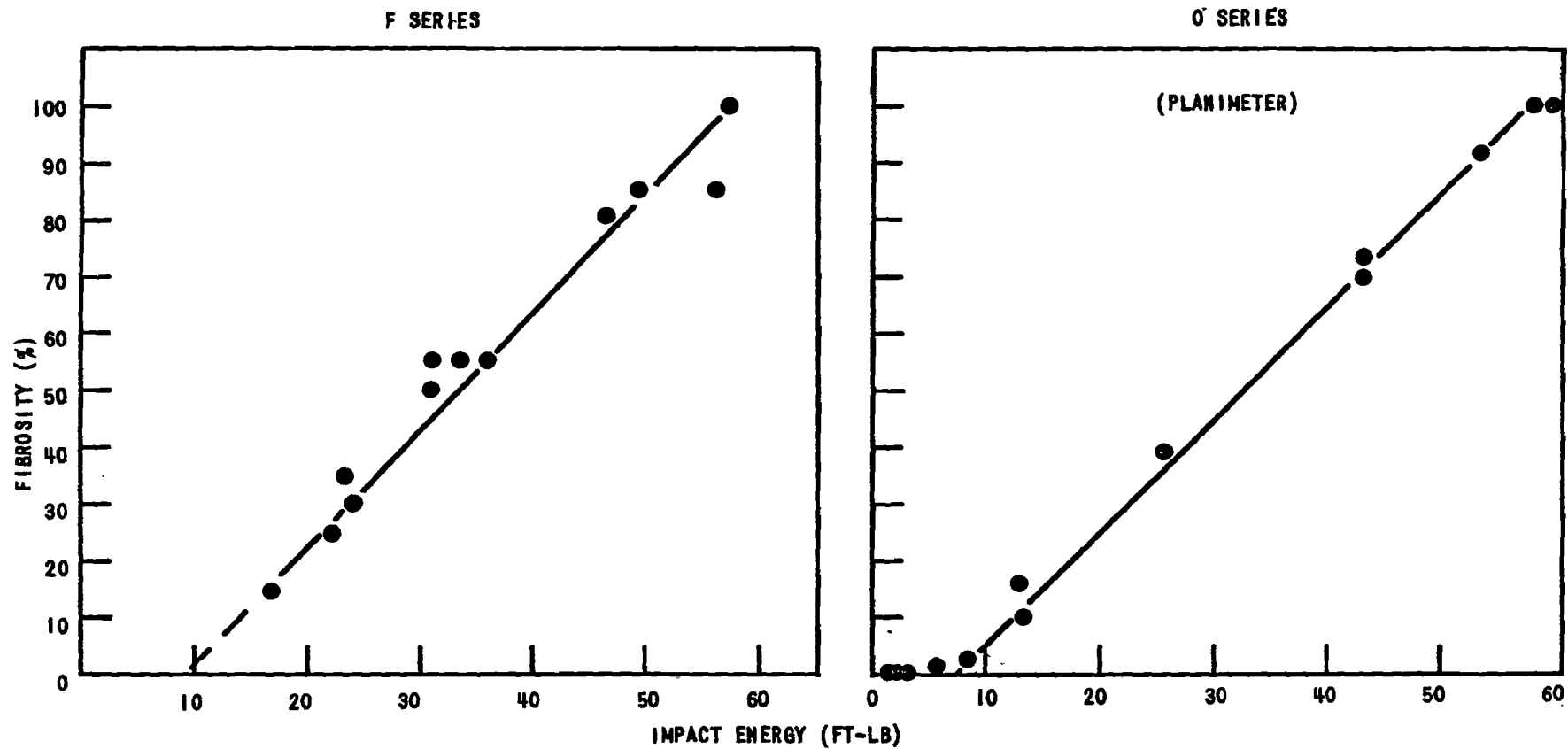
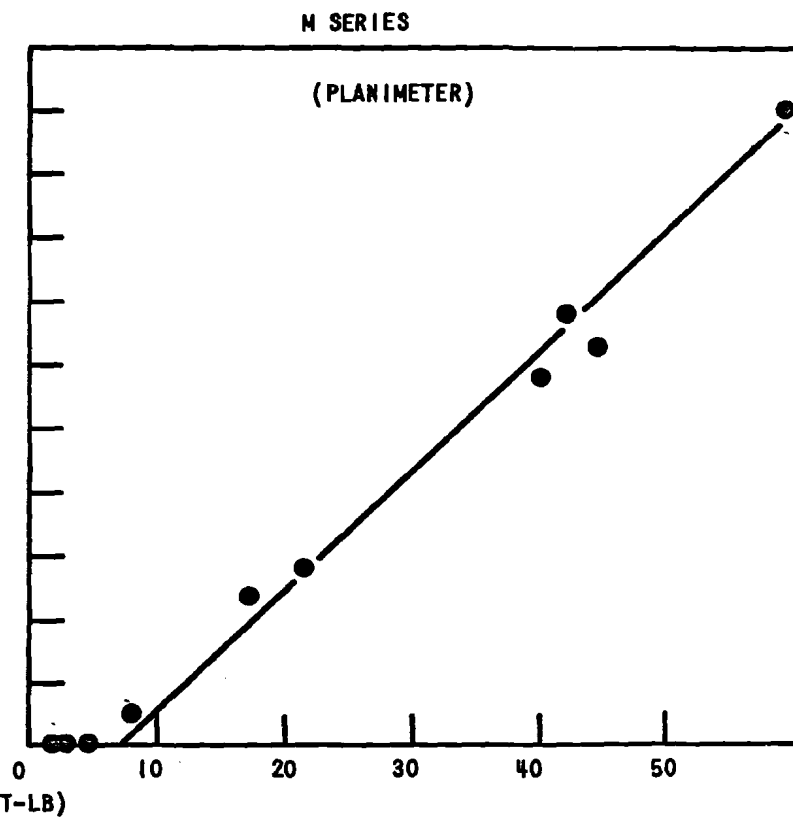
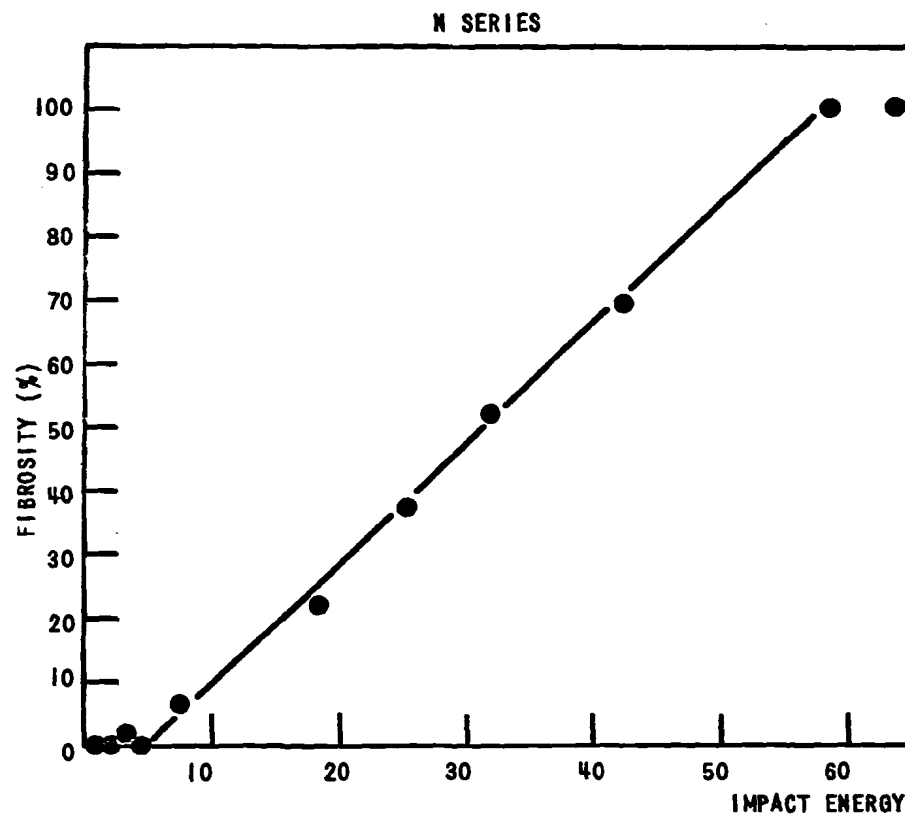


FIGURE 24



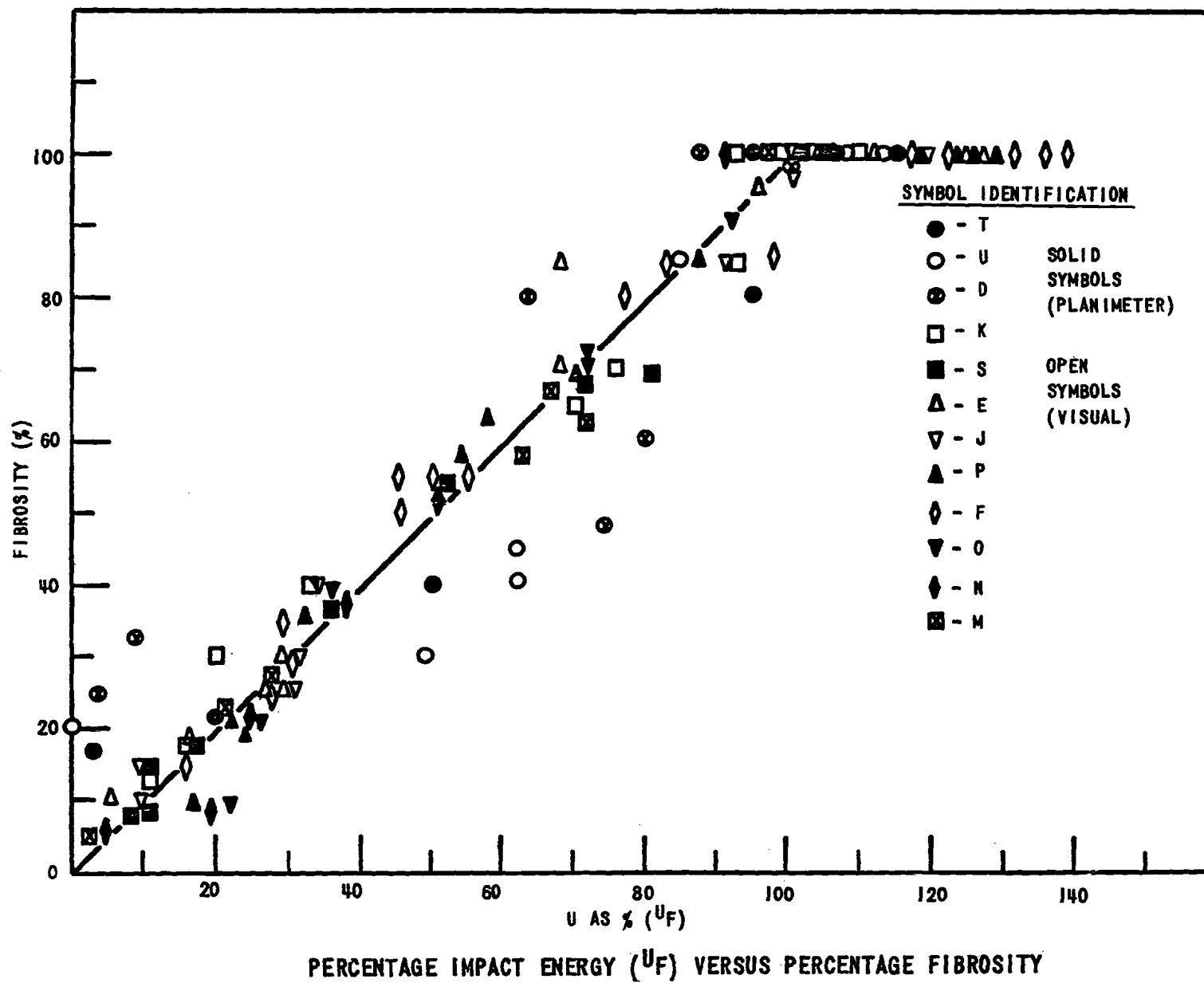
IMPACT ENERGY VERSUS FIBROSITY - SERIES F, O

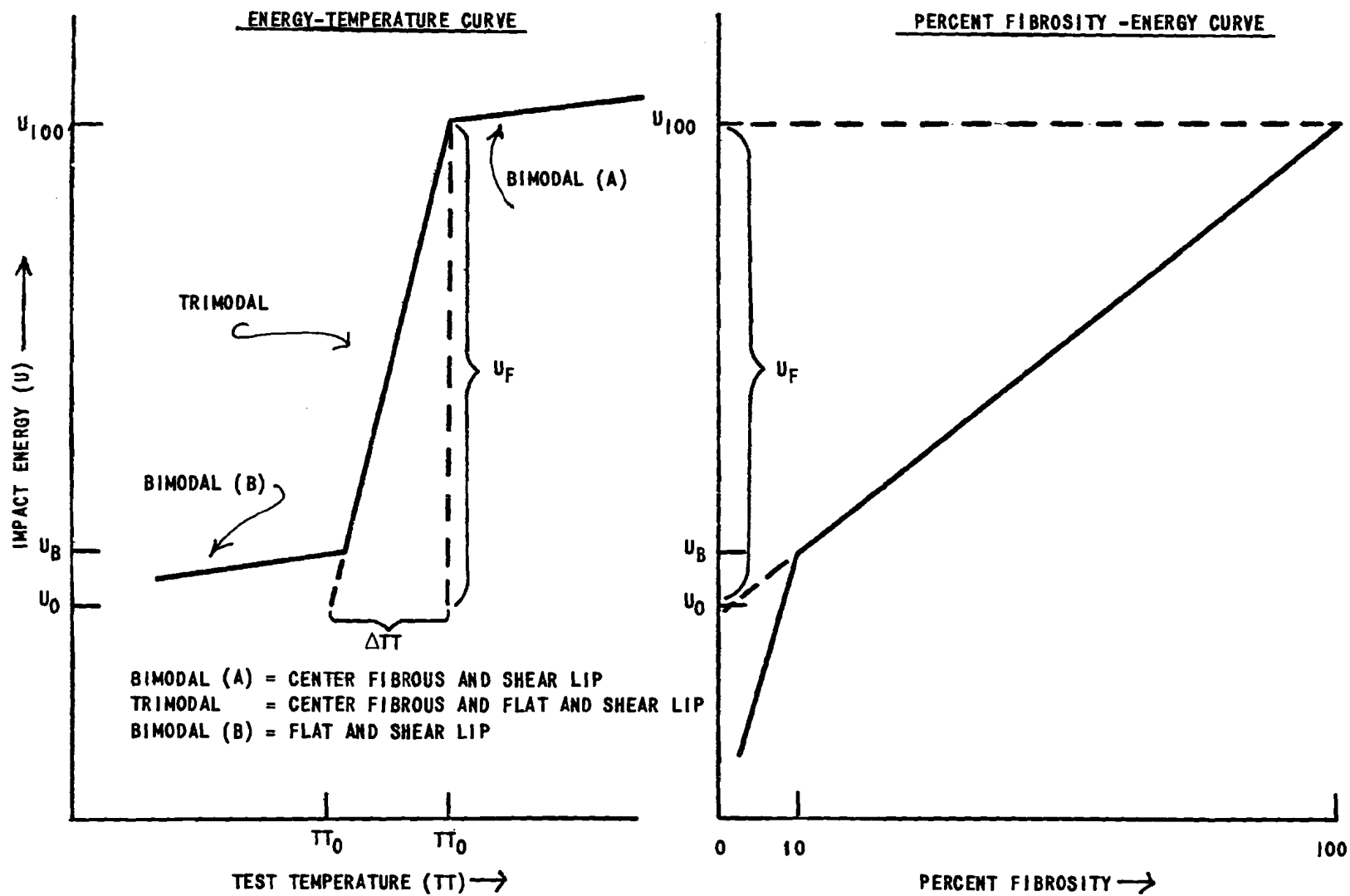
FIGURE 25



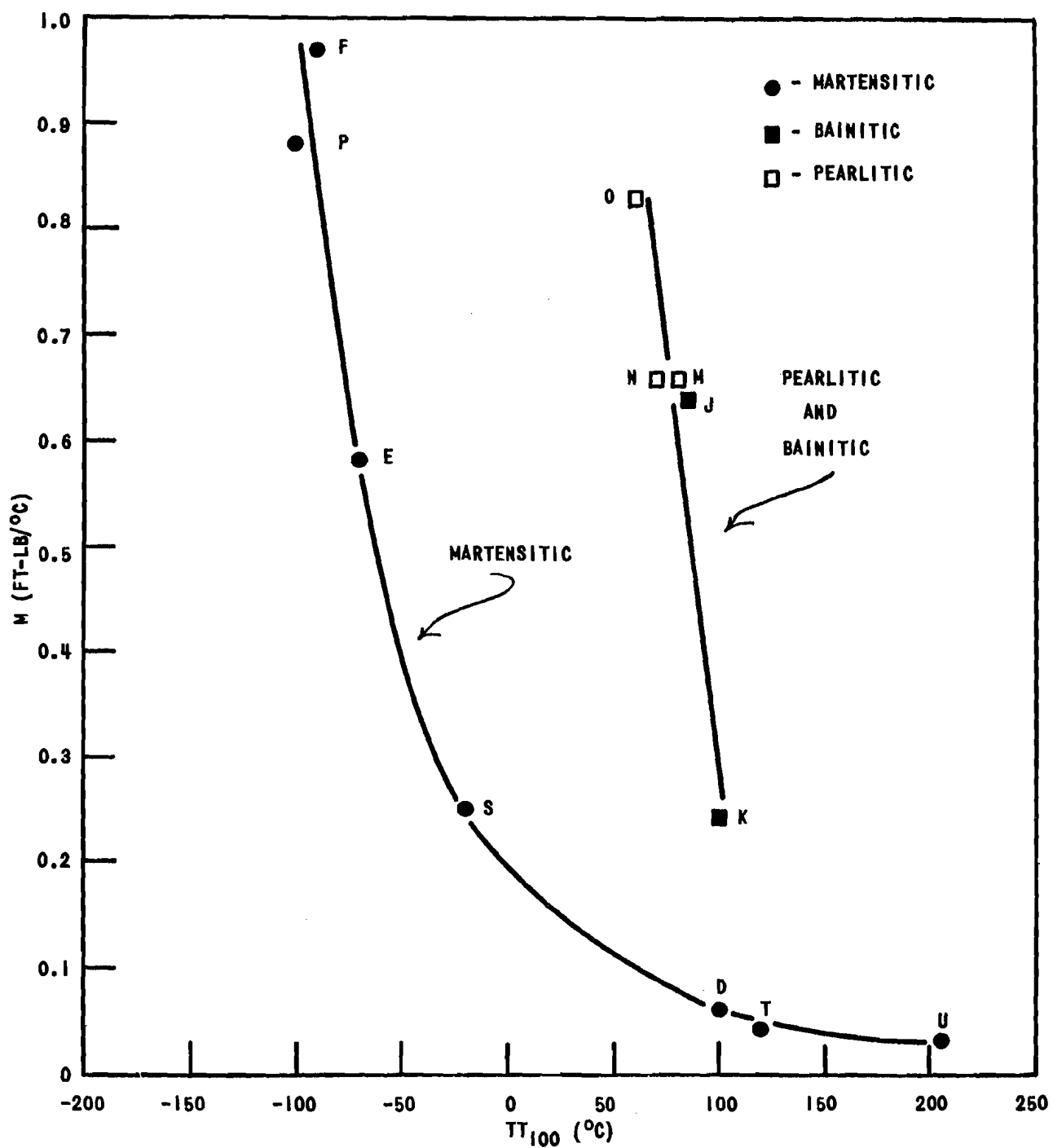
IMPACT ENERGY VERSUS FIBROSITY - SERIES N, M

FIGURE 27

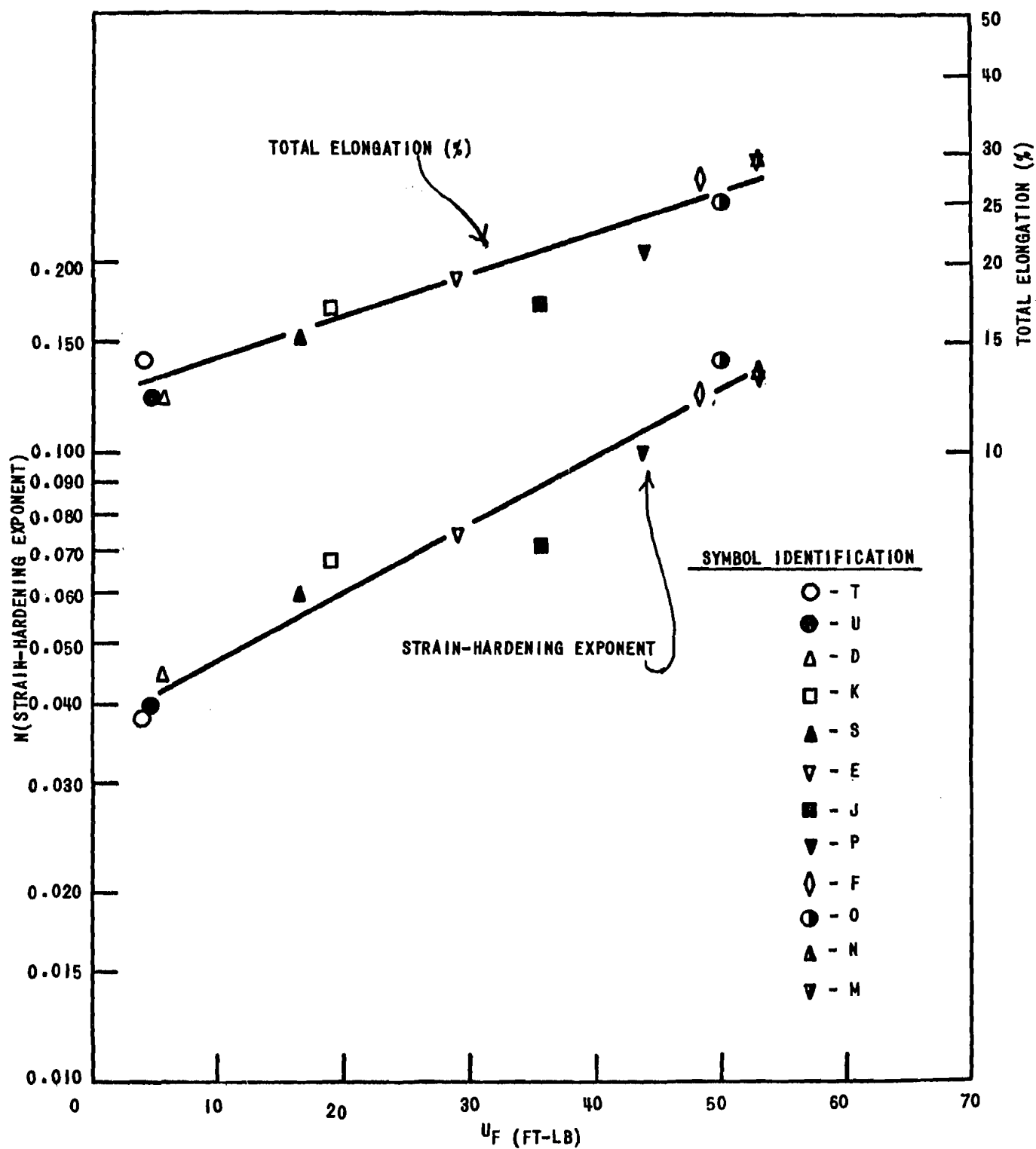




IDEALIZED CURVES OF IMPACT ENERGY VERSUS TESTING TEMPERATURE AND FIBROSITY



ENERGY-TEMPERATURE SLOPE (M) VERSUS 100% FIBROUS TRANSITION TEMPERATURE

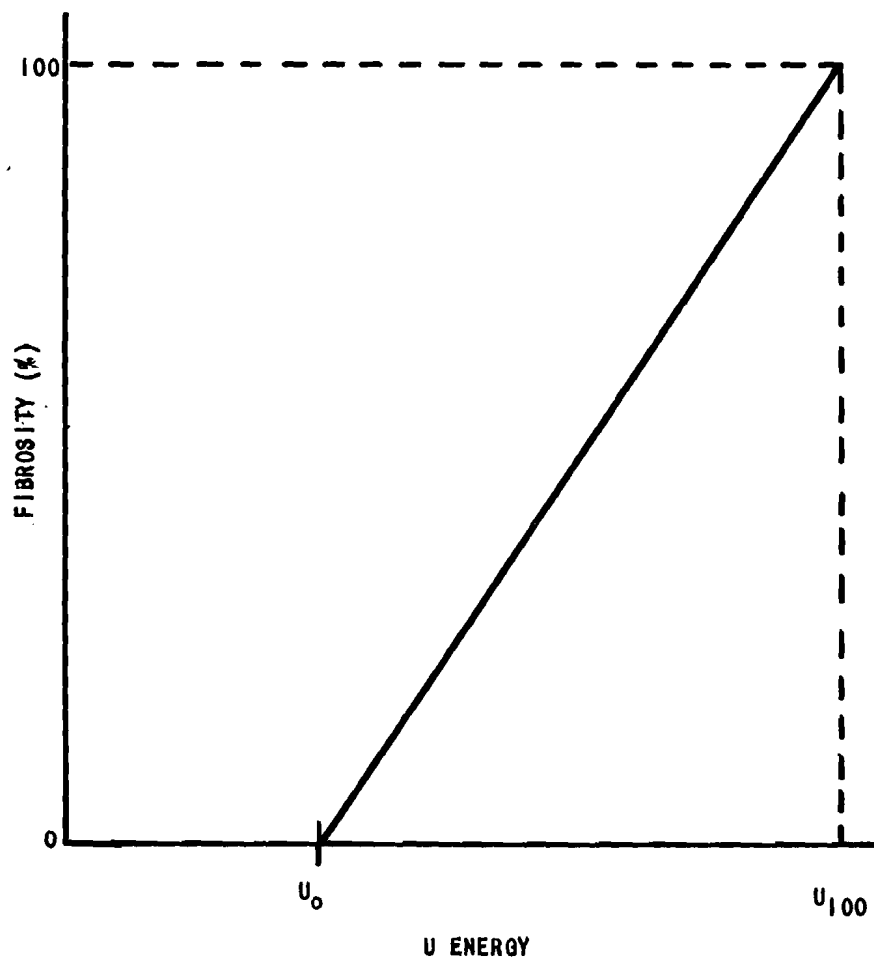


STRAIN-HARDENING EXPONENT AND DUCTILITY VERSUS IMPACT ENERGY U_F

FIGURE 30

APPENDIX A

DETERMINATION OF PERCENT ENERGY (U_F) FROM THE IMPACT ENERGY VERSUS FIBROSITY CURVES



U = IMPACT ENERGY OF ANY SPECIFIED POINT ON THE TRANSITION CURVE

U_{100} = IMPACT ENERGY AT 100% FIBROUS FRACTURE

U_0 = IMPACT ENERGY INTERCEPT AT 0% FIBROUS FRACTURE

$$U_F = U_{100} - U_0$$

$$\text{PERCENT IMPACT ENERGY } (U_F) = \frac{U - U_0}{U_F} \times 100$$

REFERENCES

1. WILLIAMS, M. L., Analysis of Brittle Behavior of Ship Plates, Symposium on Effect of Temperature on the Brittle Behavior of Metals with Particular Reference to Low Temperatures, ASTM Special Technical Publication No. 158, 1953, p.11.
2. SHANK, M. E., A Critical Survey of Brittle Failure in Carbon Plate Steel Structures other than Ships, Symposium on Effect of Temperature on the Brittle Behavior of Metals with Particular Reference to Low Temperatures, ASTM Special Technical Publication No. 158, 1953, p. 45.
3. HOLLOMON, J. H., Tensile and Impact Properties of an Alloy Steel, Watertown Arsenal Laboratory Report No. WAL 310/34, 15 September 1944.
4. MCCARTHY, D. E., and HOLLOMON, J. H., Investigation of Sub-Sized Charpy Specimen, Watertown Arsenal Laboratory Report No. WAL 112/48, 6 August 1945.
5. RANK, A. E., et al, Ductility and Fracture Resistance of Ship Plate, Naval Research Laboratory Report O-2796, 22 November 1946.
6. PARKER, E. R., Theory of Brittle Fracture and Criteria for Behavior at Low Temperatures, Symposium on Effect of Temperature on the Brittle Behavior of Metals with Particular Reference to Low Temperatures, ASTM Special Technical Publication No. 158, 1953, p. 116.
7. GROSS, J. H., and STOUT, R. D., Ductility and Energy Relations in Charpy Tests of Structural Steels, Welding Journal, Research Supplement, April 1958, p. 191-S.
8. HARTBOWER, C. E., and ORNER, G. M., Discussion to "Ductility and Energy Relations in Charpy Tests of Structural Steels", Welding Journal, Research Supplement, April 1958, p. 156-S.
9. HARTBOWER, C. E., Transition Behavior in V-Notch Charpy Slow Bend Tests, ASTM Symposium on Impact Testing, Special Technical Publication No. 176.
10. SCHEPERS, ALEXANDER, and LICHT, FRANZ-RUDOLF, Determination of Notch Toughness, Fracture Appearance and Bending Angle as Dependent on Testing Temperature, Stahl und Eisen, v. 78, no. 4, 20 February 1958, p. 227-235.
11. KORNFELD, HEINZ, Impact Strength and the Appearance of the Fracture in Notched Charpy Specimens of Normalized Plates of Unalloyed Fine-Grained Steel with an Approximate 0.15% Carbon Content, Stahl und Eisen, v. 76, 1956, p. 1173-1178.

WATERTOWN ARSENAL
WATERTOWN 72, MASSACHUSETTS

TECHNICAL REPORT DISTRIBUTION

Report No.: WAL TR 834.2/3 Title: Relationships Between Energy,
December 1961 Fibrosity and Temperature in
Charpy Impact Tests on AISI 4340
Steel

Distribution List approved by Ordnance Materials Research Office,
1 December 1960

No of
Copies

TO

10	Commander, Armed Services Technical Information Agency, Arlington Hall Station, Arlington 12, Virginia ATTN: TIPDR
1	Director, Army Research Office, Department of the Army, Washington 25, D. C.
1	Commanding Officer, Army Research Office (Durham), Box CM, Duke Station, Durham, North Carolina ATTN: ORDOR-ED
1	Chief of Ordnance, Department of the Army, Washington 25, D. C. ATTN: ORDTB, Materials
1	Commanding General, Aberdeen Proving Ground, Maryland ATTN: Ballistic Research Laboratory
3	ORDBE-LM, Technical Library, Building 313
1	Commanding General, Army Ballistic Missile Agency, Redstone Arsenal, Alabama ATTN: Dr. G. H. Reisig
1	Commanding General, Ordnance Tank-Automotive Command, Detroit Arsenal, Center Line, Michigan ATTN: ORDMC-RM.1, Mr. Charles Salter
1	Commanding General, Ordnance Weapons Command, Rock Island, Illinois ATTN: ORDOW-IX
2	ORDOW-TX
1	Commanding General, U. S. Army Ordnance Special Weapons Ammunition Command, Dover, New Jersey

No. of Copies	TO
1	Commanding General, U. S. Army Rocket and Guided Missile Agency, Redstone Arsenal, Alabama
5	ATTN: ORDAB-DV
1	ORDXR-RGA, Mr. R. L. Wetherington
1	ORDXR-RMO, Lt. E. J. Wilson
1	Commanding Officer, Detroit Arsenal, Center Line, Michigan
1	ATTN: ORDMX-BMW
1	ORDMX-AL
1	Commanding Officer, Diamond Ordnance Fuze Laboratories, Washington 25, D. C.
1	ATTN: ORDTL .012, Technical Reference Branch
2	Commanding Officer, Frankford Arsenal, Philadelphia 37, Pennsylvania
2	ATTN: Pitman-Dunn Laboratories
1	Commanding Officer, Ordnance Materials Research Office, Watertown Arsenal, Watertown 72, Massachusetts
1	ATTN: RPD
1	Commanding Officer, Picatinny Arsenal, Dover, New Jersey
1	ATTN: Feltman Research Laboratories
1	Commanding Officer, Rock Island Arsenal, Rock Island, Illinois
1	ATTN: Laboratory
1	Commanding Officer, Springfield Armory, Springfield 1, Massachusetts
1	ATTN: ORDED-TX
1	Commanding Officer, Watervliet Arsenal, Watervliet, New York
1	ATTN: ORDEF-RT
1	Chief, Bureau of Ships, Department of the Navy, Washington 25, D. C.
1	ATTN: Code 341
1	Chief, Bureau of Naval Weapons, Department of the Navy, Room 2225, Munitions Building, Washington 25, D. C.
1	ATTN: RMMP
1	Chief, Office of Naval Research, Department of the Navy, Washington 25, D. C.
1	ATTN: Code 423
1	Chief, Naval Engineering Experimental Station, Department of the Navy, Annapolis, Maryland

No. of Copies	TO
1	Commander, Naval Ordnance Test Station, China Lake, California ATTN: Code 5557
1	Director, Naval Research Laboratory, Anacostia Station, Washington, D. C. ATTN: Technical Information Officer
1	Commander, Naval Weapons Laboratory, Dahlgren, Virginia ATTN: A & P Laboratory
5	Commander, Wright Air Development Division, Wright-Patterson Air Force Base, Ohio ATTN: WWRCEE
15	U. S. Atomic Energy Commission, Office of Technical Information Extension, P. O. Box 62, Oak Ridge, Tennessee
1	Army Reactor Branch, Division of Research Development, Atomic Energy Commission, Washington 25, D. C.
1	National Aeronautics and Space Administration, 1520 H Street, N. W., Washington 25, D. C.
1	Director, Jet Propulsion Laboratory, California Institute of Technology, Pasadena 3, California ATTN: Dr. L. Jaffe
5	Dr. W. R. Lucas, George C. Marshall Space Flight Center, Huntsville, Alabama ATTN: M-S&M-M
1	Mr. W. A. Wilson, George C. Marshall Space Flight Center, Huntsville, Alabama ATTN: M-F&AE-M, Building 4720
1	Defense Metals Information Center, Battelle Memorial Institute, Columbus, Ohio
5	Commanding Officer, Watertown Arsenal, Watertown 72, Massachusetts ATTN: ORDBE-LXM, Technical Information Section
2	Authors
84	-- TOTAL COPIES DISTRIBUTED